Dynamic biomass burning emission factors and their impact on atmospheric CO mixing ratios

van Leeuwen, T. T.; Peters, W.; Krol, M. C.; van der Werf, G. R.

Published in:
Journal of geophysical research-Atmospheres

DOI:
10.1002/jgrd.50478

JOURNAL OF GEOPHYSICAL RESEARCH: ATMOSPHERES, VOL. 118, 6797–6815, doi:10.1002/jgrd.50478, 2013

Dynamic biomass burning emission factors and their impact on atmospheric CO mixing ratios

T. T. van Leeuwen,[1] W. Peters,[2] M. C. Krol,[2,3,4] and G. R. van der Werf[1]

Received 12 November 2012; revised 1 May 2013; accepted 6 May 2013; published 26 June 2013.

[1] Biomass burning is a major source of trace gases and aerosols, influencing atmospheric chemistry and climate. To quantitatively assess its impact, an accurate representation of fire emissions is crucial for the atmospheric modeling community. So far, most studies rely on static emission factors (EF) which convert estimates of dry matter burned to trace gas and aerosol emissions. These EFs are often based on the arithmetic mean of field measurements stratified by biome, neglecting the variability in time and space. Here we present global carbon monoxide (CO) emission estimates from fires based on six EF scenarios with different spatial and temporal variability, using dry matter emission estimates from the Global Fire Emissions Database (GFED). We used the TM5 model to transport these different bottom-up estimates in the atmosphere and found that including spatial and temporal variability in EFs impacted CO mixing ratios substantially. Most scenarios estimated higher CO mixing ratios (up to 40% more CO from fires during the burning season) over boreal regions compared to the GFED standard run, while a decrease (~15%) was estimated over the continent of Africa. A comparison to atmospheric CO observations showed differences of 10–20 ppb between the scenarios and systematic deviations from local observations. Although temporal correlations of specific EF scenarios improved for certain regions, an overall "best" set of EFs could not be selected. Our results provide a new set of emission estimates that can be used for sensitivity analyses and highlight the importance of better understanding spatial and temporal variability in EFs for atmospheric studies in general and specifically when using CO or aerosols concentration measurements to top-down constrain fire carbon emissions.

Citation: van Leeuwen, T. T., W. Peters, M. C. Krol, and G. R. van der Werf (2013), Dynamic biomass burning emission factors and their impact on atmospheric CO mixing ratios, *J. Geophys. Res. Atmos.*, *118*, 6797–6815, doi:10.1002/jgrd.50478.

1. Introduction

[2] The burning of biomass, human or lightning-induced, releases a large suite of trace gases and aerosols into the global atmosphere [*Crutzen and Andreae*, 1990; *Koch et al*., 2007], influencing radiative forcing agents [*Bowman et al*., 2009], interannual variability (IAV) in the growth rates of many trace gases including carbon dioxide (CO_2), methane (CH_4), and carbon monoxide (CO) [*Langenfelds et al*., 2002], plant productivity [*Sitch et al*., 2007], visibility [e.g., *Naeher et al*., 2007] and human health [e.g., *Johnston et al*., 2012].

[3] Understanding and quantifying the impact of biomass burning (BB) on atmospheric composition and chemistry requires accurate data on the emissions of trace gases and aerosols and the incorporation of fire processes in biogeochemical and dynamic global vegetation models. Combining data sets on fuel loads and satellite-derived burned area resulted in several bottom-up fire carbon (C) emission estimates [e.g., *Hoelzemann et al*., 2004; *Ito and Penner*, 2004; *van der Werf et al*., 2006]. These studies estimated an emission range between 1 and 3 Pg C yr^{-1} and showed that fires have large IAV. A research avenue that provided new constraints on these estimates were atmospheric inversions, where measurements of atmospheric trace gases in combination with chemistry transport models provide independent validation of bottom-up emission estimates [*Edwards et al*., 2004; *Arellano et al*., 2006; *Gloudemans et al*., 2006; *Kopacz et al*., 2010; *Hooghiemstra et al*., 2012a, 2012b]. In many of these inversion studies, CO is used as a tracer of fire emissions due to its relatively well-known chemistry and large departure from background conditions. The intermediate lifetime (of 2 months on average), longer than volatile compounds and aerosols emitted from fires but shorter than for example CH_4, makes CO traceable as it travels between continents [*Edwards et al*., 2004; *Gloudemans et al*., 2006]. Different satellite sensors (e.g.,

[1]Faculty of Earth and Life Sciences, VU University Amsterdam, Amsterdam, Netherlands.
[2]Department of Meteorology and Air Quality, Wageningen University, Wageningen, Netherlands.
[3]SRON Netherlands Institute for Space Research, Utrecht, Netherlands.
[4]Institute for Marine and Atmospheric Research Utrecht, Utrecht University, Utrecht, Netherlands.

Corresponding author: T. T. van Leeuwen, Faculty of Earth and Life Sciences, Earth and Climate Cluster, VU University Amsterdam, De Boelelaan 1085, Rm. E-344, 1081 HV Amsterdam, Netherlands. (t.t.van.leeuwen@vu.nl)

2169-897X/13/10.1002/jgrd.50478

Measurements of Pollution in the Troposphere [MOPITT], Tropospheric Emission Spectrometer, and the Atmospheric Infrared Sounder) are able to measure CO column concentrations and also a relatively long and consistent time series of CO from the National Oceanic and Atmospheric Administration (NOAA) Cooperative Air Sampling Network exists [*Novelli et al*., 1998, 2003].

[4] While our knowledge on the spatial and temporal variability of fires substantially increased in the last decade due to new satellite information, several important gaps remain in our understanding of BB emissions. During the last years, new burned area products have been developed, and validation studies indicated that the Moderate Resolution Imaging Spectrometer products [*Roy et al*., 2008; *Giglio et al*., 2009] identify the majority of area burned as estimated by Landsat-derived burned area [*Roy and Boschetti*, 2009; *Giglio et al*., 2010]. However, the burned area algorithms have difficulty in mapping small fires [*Randerson et al*., 2012] as well as understory fires or fires that burn during periods with persistent cloud cover. The conversion of burned area to fire emissions also bears uncertainties; the large variability in fuel consumption often reported by field measurements studies, especially in heterogeneous landscapes, is difficult to extract from satellite data [*van der Werf et al*., 2010].

[5] Another important source of uncertainty is the partitioning of combusted biomass or C into different combustion products. To translate the fire C losses to trace gases and aerosols, emission factors (EFs) are used. An EF is usually defined as the amount of a specific trace gas emitted per kg of dry matter (DM) burned, expressed in units of g kg^{-1} DM^{-1} [*Andreae and Merlet*, 2001]. Since the launch of the first BB campaigns back in the 1980s, EFs have been measured in most fire-prone biomes. Several summaries of experimental EF data were given [e.g., *Delmas et al*., 1995], but the most extensive and frequently used database of all EF measurements was compiled by *Andreae and Merlet* [2001] with annual updates (M.O. Andreae, personal communication 2011). Recently, *Akagi et al*. [2011] compiled a new EF database and only included measurements of fresh plumes, which adds consistency especially for volatile compounds. Most modeling studies have used EFs based on the arithmetic mean of field measurement outcomes, stratified by biome, and taken from the EF compilations mentioned above. This approach cannot account for the variability in EFs within biomes, which can be substantial. In general, natural variability in fuel moisture, fuel geometry, topography, and wind speed causes variability in the ratio of biomass consumption by flaming and smoldering combustion [*Hely et al*., 2003; *McMeeking et al*., 2009; *Chen et al*., 2010]. This, coupled with variations in chemical composition of the fuel, leads to a substantial range in the naturally occurring EFs for different species and fire types [*Akagi et al*., 2011]. This variability is usually not taken into account in large-scale emission estimates except for variations due to vegetation type. In addition to the lack of representation in spatiotemporal variability, the often-used averaged EFs may have limitations because it is not known whether they are based on a representative sample for various biomes [*van Leeuwen and van der Werf*, 2011].

[6] To assess the temporal variability of EFs, *Korontzi et al*. [2003a, 2003b] conducted field measurements in African grassland fires over one fire season. Relatively high CO and CH_4 EFs were found in the beginning of the dry season, and lower EFs were measured toward the end of the dry season. Similar types of studies in southern Africa supported these findings [*Hoffa et al*., 1999; *Korontzi et al*., 2004; *Korontzi*, 2005]. A study of *Meyer et al*. [2012] found no evidence for a significant seasonality in CH_4 EFs in Australian bushfires but indicated that variation in EFs across vegetation and fuel types is substantial and needs to be considered in emission assessments. The latter was confirmed by *Wooster et al*. [2011], who conducted measurements in late dry season fires in southern Africa: a range of 68–127 g kg^{-1} for CO EF was found for burning plots containing different proportions of savanna fuel types.

[7] So far, only a few regional emissions modeling studies considered seasonal and/or spatial variability of EFs. *Hoffa et al*. [1999] and *Korontzi* [2005] used the proportion of green grass biomass to total (green + dead) grass biomass to model fire emissions in southern African savannas. Partly building on the work of *Hoffa et al*. [1999], *Ito and Penner* [2005] applied three different methods for determining EFs to estimate CO emissions from open BB in southern Africa. All studies demonstrated that regional emission estimate outcomes were dependent on the variable EFs used: differences in fire CO emission estimates over 50% were found when comparing seasonally variable EFs versus fixed EFs [*Korontzi*, 2005]. The impact of fuel type–specific CH_4 EFs in Australian bushfires was shown by *Meyer et al*. [2012], who compared the use of one single EF for CH_4 with EFs specified for separate fuel types in a sensitivity analysis. Introducing a separate EF for smoldering logs resulted in a 15% increase of total emissions over 2003–2009. On the other hand, an emission reduction of 21% was found when assigning a separate EF for fine logs.

[8] Here we developed six EF scenarios for CO using different methods to model their spatial and temporal variability. The scenarios were implemented in a bottom-up modeling framework, and the resulting emissions were transported with the TM5 atmospheric tracer model. We focus on CO but because its EF correlates reasonably well with several other trace gases and aerosols, this work can be expanded to other species. We show results for the years 2002–2007 to capture multiple anomalous BB events including large boreal fires in Siberia and Alaska in 2003 and 2004 and high fire episodes in the Cerrados (savannas) and deforestation regions of Brazil in 2007. The focus on this time period allowed for a comparison with several recently published inversions as well. Our main objective was to understand the impact of spatial and temporal variability in EFs on large-scale emission assessments and provide the CO modeling community with new information on the construction and use of EF scenarios in BB emission estimates.

2. Methods

[9] An overview of the modeling framework that was used to estimate bottom-up emissions of CO is given in section 2.1. We transported the CO emission fields using the TM5 atmospheric transport model, which is further explained in section 2.2. In section 2.3, we describe the flask observations and satellite-based measurements that were used in the model-data comparison.

Table 1. Overview of the Different EF Scenarios Implemented in the GFED Modeling Framework, Currently Using the GFED-A&M Scenario

EF Scenario	EF Data Set	Temporal Variability	Spatial Mapping
GFED-A&M	[*Andreae and Merlet*, 2001][a]	No	0.5°, 6 biomes
GFED-AKAGI	[*Akagi et al*., 2011]	No	0.5°, 8 biomes
ENVI-A&M	[*Andreae and Merlet*, 2001]	Monthly	0.5°
ENVI-AKAGI	[*Akagi et al*., 2011]	Monthly	0.5°
MCE-STATIC	–	No	0.5°, 7 fuel types
MCE-SEASON	–	Monthly	0.5°, 7 fuel types

[a]EF database of [*Andreae and Merlet*, 2001], including annual updates till 2011.

2.1. Bottom-Up Emission Estimates of CO

[10] Bottom-up fire emissions were taken from the Global Fire Emissions Database version 3 (GFED3: *Giglio et al*., 2010; *van der Werf et al*., 2010). The data set consists of 0.5° × 0.5° monthly fields of burned area, fuel loads, combustion completeness, and fire C losses. Fire emissions were estimated based on burned area [*Giglio et al*., 2010], and the satellite driven Carnegie-Ames-Stanford Approach (CASA) biogeochemical model was used to calculate fuel loads and combustion completeness [*van der Werf et al*., 2010]. CASA calculates for every grid cell and every time step C pools, based on C input from net primary production and C losses through heterotrophic respiration, herbivory, fuelwood collection and fires. More details on the modeling framework can be found in *van der Werf et al*. [2010]. The focus of this study is on the conversion of C losses into different trace gas emissions, in our case CO. In the subparagraphs below, a description is given of the different EF scenarios we applied in this study, which are summarized in Table 1.

2.1.1. GFED-A&M

[11] GFED-*Andreae and Merlet* [2001] (abbreviated as GFED-A&M in the remainder of the paper) corresponds to the EF scenario that was used in GFED3 [*van der Werf et al*., 2010]: Biome-averaged EFs, compiled by *Andreae and Merlet* [2001] and updated annually by M. O. Andreae (2011, personal communication) were derived from measurements of fires in tropical forest, savanna and grassland, extratropical forest, tropical peat, and agricultural area. For tropical peat burning in Indonesia only one measurement [*Christian et al*., 2003] was used to estimate the CO EF, which was about twice as high as the EF for tropical forest fires. The average EF of tropical forest and savanna/grassland fires was applied to woodland fires because they represent a mixture of these fire types. The extratropical forest biome consists of all EF measurements made in the boreal and temperate zone. An overview of the CO EFs for the different biomes is given in Table 2. No temporal variability for the biome-averaged EFs was taken into account in the GFED-A&M scenario; e.g., a fire in the early dry season was given the same CO EF as a fire during the end of the dry season.

2.1.2. GFED-AKAGI

[12] The GFED-*Akagi et al*. [2011] (AKAGI) scenario followed a similar approach as GFED-A&M but used biome-averaged EF values of the more recent compilation of *Akagi et al*. [2011]. In contrast to the EF database of *Andreae and Merlet* [2001], *Akagi et al*. [2011] used EF measurements of "fresh" smoke plumes only. These fresh plumes have cooled to ambient temperature, but have not yet undergone significant photochemical processing. Since chemical disturbances are therefore neglected, they may allow for a better representation of the true regional initial emissions of a fire. This is not crucial for CO, but for more volatile gases, it may have a large impact on measured EFs. Besides a reduction in the amount of field studies used (Table 2), the database of *Akagi et al*. [2011] also used a different and more extensive partitioning of EFs into different biomes. Selected EFs for landscape scale fires were organized into six types of vegetation: savanna, tropical forest, boreal forest, temperate forest, peatland, and chaparral. Thus, the category extratropical forest used by *Andreae and Merlet* [2001] was divided into boreal and temperate forest. *Akagi et al*. [2011] used a weighted average of boreal and temperate EFs (86.5% and 13.5%, respectively) for extratropical forest fires, based on GFED3 biomass consumption estimates [*van der Werf et al*., 2010].

Table 2. Biome-Averaged CO EFs in g kg^{-1} DM^{-1} for the GFED-A&M and GFED-AKAGI Scenario[a]

	GFED-A&M		GFED-AKAGI	
Biome	EF CO	*n*	EF CO	*n*
Tropical Forest	100 (±16)	15	93 (±27)	5
Savanna & Grassland	64 (±20)	35	63 (±17)	5
Chaparral	–	–	67 (±13)	3
Woodland[b]	82 (−)	–	94.5 (−)	–
Extratropical Forest	110 (±40)	32	122 (±44)	–
Boreal Forest	–	–	127 (±45)	9
Temperate Forest	–	–	89 (±32)	3
Peatland[c]	210 (−)	1	210 (−)	1
Agricultural Area	95 (±68)	16	102 (±33)	2

[a]The standard deviation (SD) is shown in parenthesis, and *n* corresponds to the number of EF studies used.
[b]Woodland EF values were defined as the average EF for the tropical forest and the savanna and grassland biomes, and therefore the number of studies (*n*) and standard deviation (SD) were not given.
[c]Peatland EF values were the same for both scenarios and based on field measurements of *Christian et al*. [2003].

Table 3. Correlation Coefficients (r) and F Values for CO EF Measurements and Various Environmental Data Sets, Based on Two Scenarios: ENVI-A&M and ENVI-AKAGI[a]

	ENVI-A&M ($n = 233$)		ENVI-AKAGI ($n = 104$)	
Driver Data	r	F Value	r	F Value
Fraction tree cover	0.46	63.5	0.4	19.6
Mean monthly precipitation	0.32	25.9	0.34	12.9
Mean annual precipitation	0.08	*1.3*	0.19	3.8
Mean monthly temperature	−0.06	*0.7*	0.11	*1.1*
Mean annual temperature	−0.29	21.5	−0.07	*0.6*
NDVI	0.44	57.0	0.48	30.2
Length dry season	0.07	*1.3*	−0.04	*0.2*
r Combined	0.53	89.9	0.53	40.7

[a]The correlation coefficient for the multivariate regression equation is also shown (r combined). n corresponds to the number of EF measurements used, and F values shown in italic indicate relations that did not exceed the critical F value for a significance level of 0.01.

[13] For peatland EFs we made the following assumption: since the GFED modeling framework only takes peatlands in Indonesia into account, we excluded the peat measurements for boreal North America used by *Akagi et al*. [2011]. Therefore, the CO EF for peatland was based on one study for Indonesia, the same study that was used for the GFED-A&M scenario. EF measurements in chaparral vegetation, a type of shrubland that is primarily found in California (US) and in the northern portion of the Baja California peninsula (Mexico), were used to define an average EF for this biome: In the 30°N–40°N, 70°W–55°W region, the savanna and grassland EFs were replaced by the biome-averaged EFs values for chaparral, which are slightly higher (~6%) than those for the savanna and grassland biome. In the GFED-AKAGI scenario, just like GFED-A&M, no temporal variability for the biome-averaged EFs was taken into account.

2.1.3. ENVI-A&M

[14] In addition to the spatial variability related to the distribution of different biomes, EFs may also show some degree of seasonal variation. During relatively moist conditions in the early fire season, the smoldering-flaming ratio is expected to be higher, leading to higher CO EFs. On average, toward the end of the dry season, a decrease in fuel moisture may result in a more complete flaming combustion (well-oxidized), resulting in lower CO EFs [*Hoffa et al*., 1999; *Hely et al*., 2003; *Korontzi et al*., 2003a, 2003b]. This seasonal variation is not taken into account in the GFED-A&M and GFED-AKAGI scenarios, but we did include a temporal component in the ENVI-A&M scenario described here.

[15] Only a few measurements of the seasonal variation of EFs are available, so we build on our previous modeling work to assess the seasonal variability of EFs for different biomes. Relations between EF measurements from the *Andreae and Merlet* [2001] database (including annual updates till 2011) and different measurements of environmental variables that may correlate with part of the variability in EFs—including fraction tree cover (FTC), normalized difference vegetation index (NDVI), mean annual precipitation, mean monthly precipitation, mean annual temperature, mean monthly temperature, and the length of the dry season—were explored in *van Leeuwen and van der Werf* [2011]. To assess what fraction of the variability in CO EF measurements was correlated with coarse-resolution global environmental data sets, we applied linear regressions between the CO EF values and environmental parameters corresponding to the EF measurement locations (Table 3). We refer the reader to *van Leeuwen and van der Werf* [2011] for a more extensive description of the different environmental data sets used and the statistical methods that were applied.

[16] Global CO EF fields with a spatial resolution of 0.5° × 0.5° and a temporal resolution of 1 month were estimated by combining all environmental data sets in a multivariate regression equation for CO ($r = 0.53$, $F = 89.9$) with the data sets ranked in order of importance.

$$\begin{aligned}\text{CO EF} = {} & 54.710 + 0.6106 \times \text{FTC} + 0.015 \times \text{NDVI} \\ & + 0.0041 \times \text{MMP} - 0.7884 \times \text{MAT} + 0.0019 \\ & \times \text{MAP} + 0.8577 \times \text{LDS} + 0.4221 \times \text{MMT}\end{aligned} \quad (1)$$

[17] Note that data sets with low correlations coefficients ($r < 0.1$) were included in the multivariate regression, but automatically played a minor role in the equation. CO EF fields for peatlands in equatorial Asia were given the same values as the GFED-A&M scenario, since EF measurements from peat were not taken into account in the linear regressions; peatlands showed often very high CO EF values that were not related to any of the environmental parameters described above and were outliers in the equation.

2.1.4. ENVI-AKAGI

[18] In the ENVI-AKAGI scenario, we made the same assumptions as for ENVI-A&M, but we now used the EF data set of *Akagi et al*. [2011] to find relations between CO EFs and the different environmental parameters (Table 3). The lower number of measurements led to a somewhat different equation but again NDVI ($r = 0.48$, $F = 30.2$) and FTC ($r = 0.40$, $F = 19.6$) were contributing the most to the EF variability. The multivariate regression equation used to calculate the global CO EF fields ($r = 0.53$, $F = 40.7$) is:

$$\begin{aligned}\text{CO EF} = {} & -11.0296 + 0.0577 \times \text{NDVI} + 0.1204 \times \text{FTC} \\ & + 0.0911 \times \text{MMP} + 0.1761 \times \text{MAP} + 1.0854 \\ & \times \text{MMT} - 0.324 \times \text{MAT} + 4.5213 \times \text{LDS}\end{aligned} \quad (2)$$

[19] For reasons explained in section 2.1.3, we used the same CO EF values for peatlands in equatorial Asia as in the GFED-AKAGI scenario.

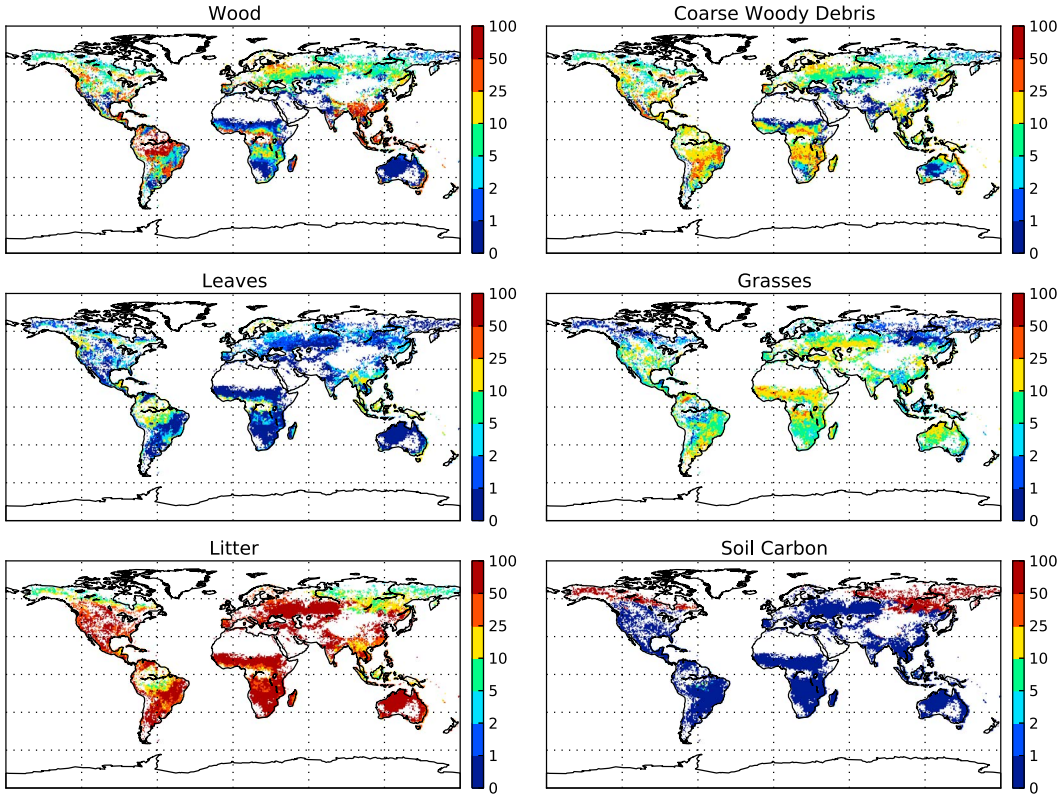

Figure 1. Fraction (%) of total carbon (C) combusted by specific fuel types in the CASA-GFED biogeochemical-modeling framework, based on the 2002–2007 weighted mean.

2.1.5. Modified Combustion Efficiency (MCE)-STATIC

[20] The MCE-STATIC scenario differs from the first four scenarios, and is together with MCE-SEASON (section 2.1.6) the most experimental. CO EFs were estimated using the Modified Combustion Efficiency (MCE), defined as the fraction of molar-based CO_2 and CO emissions that is emitted as CO_2 [*Ward et al.*, 1996; *Ferek et al.*, 1998]. The MCE is useful to indicate the relative amount of flaming and smoldering combustion during a fire, and different fuel types are assumed to have different MCEs. Laboratory experiments have shown that MCE ranges from near 0.99 for flaming combustion to ~0.65–0.85 for smoldering combustion [*Yokelson et al.*, 1996], although in general, smoldering combustion has an MCE of about 0.8 [*Akagi et al.*, 2011].

[21] Following the findings of *Meyer et al.* [2012] that variation in EFs across fuel types is important, we predefined MCEs for seven different fuel types: wood, coarse woody debris, leaves, grasses, litter, soil C, and peat based on literature data when available. Note that this distinguishes the MCE approach from the others. An overview of the fraction of C that is combusted by each of these specific fuel types is shown in Figure 1. The GFED modeling framework indicates substantial variability in the contribution of the different fuel types; in boreal regions, soil C contributes most to emissions in the model, while litter is the largest contributor in midlatitude forests and savannas. Wood only dominates (sub)tropical forests.

[22] Fuel type–specific MCEs reported in the literature vary to a large degree, and in Table 4, an overview is given of the literature. The MCEs we used in the MCE-STATIC scenario were grid cell specific but did not change seasonally. We aimed to define an MCE that was typically found during the end of the local dry season, the period of the year where in many regions of the world, fire emissions are highest.

[23] Since wood as in standing trees in general does not burn but is mostly a fuel component in deforestation regions, where it is often cut, dried, and then burned, we assumed wood to have the same MCE as coarse woody debris (CWD), which includes large logs and branches. The MCE for both fuel types was set to 0.89. Higher MCEs are normally found for fuel types with a larger surface to volume ratio, like grasses, leaves, and litter, including small twigs, branches, and downed leaves. Leaves—still attached to the tree or shrub—were given an MCE of 0.92, and grasses a slightly higher MCE (0.95). Litter often shows a large range in MCEs, and we set the value to 0.96 thought to correspond to an end of the dry season value. Soil C, including the duff layer, is assumed to burn more in the smoldering phase and thus with a lower MCE (0.85). Since peat is only defined in GFED3 in equatorial Asia, we used the measurements of *Christian et al.* [2003] to set an MCE of 0.83 for the burning of peat.

[24] Using these predefined MCEs for each fuel type, we developed global and monthly variable MCE fields by weighing the MCEs of the different fuel types in each grid cell by their relative contribution to total emissions. Since the MCE indicates the relative amount of flaming and smoldering combustion, it often correlates well with EFs of other trace gases and aerosols [*Yokelson et al.*,

Table 4. Overview of Seven Different Fuel Types That Were Defined in the CASA-GFED Biogeochemical Model, and Their MCE and MCE Range for the MCE-STATIC and MCE-SEASON Scenario, Respectively[a]

Fuel Type	MCE-STATIC	MCE-SEASON	Memory (%)	Literature Used
Wood	0.89	0.83–0.90	40	*Goode et al*., [1999]
Coarse woody debris	0.89	0.83–0.90	40	*Goode et al*., [1999], *Bertschi et al*., [2003]
Leaves	0.92	0.88–0.93	10	*Chen et al*., [2010]
Grasses	0.95	0.90–0.96	10	*Yokelson et al*., [1996], *Goode et al*., [1999], *Christian et al*., [2003], *McMeeking et al*., [2009], *Chen et al*., [2010], *Burling et al*., [2010], *Burling et al*., [2011]
Litter	0.96	0.86–0.97	10	*Yokelson et al*., [1996], *Yokelson et al*., [2008], *Yokelson et al*., [2011], *Goode et al*., [1999], *Korontzi et al*., [2003b], *Bertschi et al*., [2003], *Christian et al*., [2003], *Chen et al*., [2010], *McMeeking et al*., [2009], *Burling et al*., [2010], *Burling et al*., [2011]
Soil C	0.85	0.80–0.86	30	*Yokelson et al*., [1997], *Bertschi et al*., [2003], *McMeeking et al*., [2009], *Chen et al*., [2010], *Burling et al*., [2010]
Peat	0.83	0.81–0.85	30	*Christian et al*., [2003]

[a]The memory function—the contribution of the previous month's MCE (%)—is also shown. The last column shows the literature that was used to define the MCE range.

2003; *Janhaell et al*., 2010]. According to the EF database of *Andreae and Merlet* [2001], based on 186 measurements conducted in different biomes, the following relation between MCE and CO EF exists:

$$\text{CO EF} = -1070.7 \times \text{MCE} + 1075.1 \left(r^2 = 0.98, n = 186\right) \quad (3)$$

[25] According to the EF database of *Akagi et al*. [2011], based on 104 measurements, this relation is:

$$\text{CO EF} = -1082.7 \times \text{MCE} + 1086.5 \left(r^2 = 0.99, n = 104\right) \quad (4)$$

[26] These equations are very similar, and differences between CO EF fields when using equations (3) and (4) were negligible. We used equation (3) to estimate global and monthly variable CO EF fields, because it was derived from a larger sample of measurements.

2.1.6. MCE-SEASON

[27] Instead of defining a specific MCE as in MCE-STATIC, in the MCE-SEASON scenario we assumed MCE to vary between a set minimum and maximum MCE for the different fuel types. The MCE was scaled within this predefined range following a similar approach that is used in GFED to scale the combustion completeness based on the difference between potential evapotranspiration and monthly precipitation as a proxy for the dryness of the fuel.

[28] An overview of literature used to define MCE ranges for MCE-SEASON is given in Table 4, and these were used to set the MCE: Wood and CWD were given the same MCE range starting at 0.83 (wet) to 0.90 (dry). For leaves that are still attached to the tree or shrub, we defined a range of 0.88–0.93. The range for grasses was set slightly higher following published values (Table 4), with a minimum of 0.90 and a maximum of 0.96. Litter has a large range in MCE with values of ~0.80 in boreal areas for pure smoldering fires (R.J. Yokelson, personal communication 2011). We set the range to 0.86–0.97 to reflect the large variability, although we set the minimum higher to account for the fact that fires are rarely 100% smoldering. Soil C was given a minimum and maximum MCE value of 0.80 and 0.86, respectively, and for peat a range of 0.81–0.85 was defined to add a seasonal variation to the emissions.

[29] Similar to the approach used in CASA to model combustion completeness, we included some degree of memory by not just taking environmental conditions of the month when fires occurred but we also took the conditions in the previous month into account. These contributions (%) for the different fuel types can be found in Table 4. We assumed that wood and CWD were more affected by previous month's conditions since these fuel types are coarser and require more time to dry. Therefore, the contribution of previous month's MCE was set to 40%. Leaves, grasses, and litter have a larger surface to volume ratio and are therefore less affected by previous environmental conditions; these fuel types can dry relatively easy and were given a contribution of 10%. For soil C and peat, these effects were assumed to be larger, up to 30%.

[30] Although we acknowledge that both MCE-SEASON and MCE-STATIC scenarios are highly experimental and heavily based on expert judgments, we feel that it presents an alternative to the other scenarios with some appealing features that are based on our (limited) understanding of burning dynamics. In addition, this approach can be relatively easily ingested in emissions modeling frameworks.

2.2. TM5 Atmospheric Transport Model

[31] To simulate atmospheric CO column mixing ratios, we transported the GFED CO emissions—based on the different EF scenarios—through the atmosphere using the TM5 tracer model [*Krol et al*., 2005; *Huijnen et al*., 2010]. TM5 is an offline model driven by 3-hourly meteorological fields from the European Centre for Medium-Range Weather Forecasts (ECMWF), using ECMWF Re-Analysis (ERA)-Interim meteorological fields on a subset of 25 of the originally 60 hybrid ECMWF layers. The model runs on a coarse $2^\circ \times 3^\circ$ (latitude × longitude) horizontal grid and deviates from the typical full chemistry version by using only a subset of the available chemistry to calculate CO distributions efficiently. We used a simplified CO-OH chemistry scheme in which the hydroxyl radical (OH) is prescribed based on a rescaling (with a factor 0.92) of the *Spivakovsky et al*. [2000] distributions to match methylchloroform decay rates [*Huijnen et al*., 2010] and with CO + OH loss rates as in *Huijnen et al*. [2010]. The removal of CO by dry deposition is included, as well as production of CO from the oxidation of nonmethane volatile organic

Table 5. Overview of Annual Emission Estimates (Tg CO yr^{-1}) for Different Regions in the World, Spatially Defined as in Figure 2[a]

Region[b]	GFED-A&M	GFED-AKAGI	ENVI-A&M	ENVI-AKAGI	MCE-STATIC	MCE-SEASON	Mean	SD	Difference
BONA	16.10	18.79	15.72	16.03	21.04	22.32	18.33	2.85	+13.87
TENA	2.05	1.80	1.89	1.89	1.79	2.04	1.91	0.11	−6.83
CEAM	3.51	3.25	3.24	3.62	3.39	3.61	3.44	0.17	−2.09
NHSA	3.83	3.58	3.90	4.56	3.87	4.02	3.96	0.33	+3.39
SHSA	62.62	58.25	62.24	68.63	67.25	69.26	64.71	4.35	+3.33
EURO	0.83	0.77	0.76	0.79	0.74	0.79	0.78	0.03	−6.02
MIDE	0.33	0.32	0.26	0.29	0.22	0.22	0.27	0.05	−17.17
NHAF	69.75	66.34	68.71	66.32	66.93	63.01	66.84	2.33	−4.17
SHAF	87.51	82.21	86.60	82.49	84.83	81.03	84.11	2.61	−3.88
BOAS	26.68	30.54	26.03	24.67	36.41	39.55	30.65	6.09	+14.87
SEAS	6.32	6.26	6.08	6.10	6.69	7.90	6.56	0.69	+3.77
CEAS	20.60	19.27	19.53	20.49	21.15	21.04	20.35	0.78	−1.23
EQAS	47.43	48.80	46.97	49.38	45.87	47.53	47.66	1.27	−0.49
AUST	19.63	18.41	19.19	22.39	18.09	16.95	19.11	1.86	−2.65
Global	367.18	358.59	361.19	367.64	378.28	379.26	368.69	8.55	+0.41

[a]Results are shown for six different EF scenarios, based on the 2002-2007 average. Columns 8-10 show, respectively, the mean emission estimate (Tg CO yr-1) for the six EF scenarios, the standard deviation (SD), and the difference (%) of the mean emission estimate compared to the EF scenario that is currently used in GFED3 (GFED-A&M).

[b]BONA = Boreal North America, TENA = Temperate North America, CEAM = Central America, NHSA = Northern Hemisphere South America, SHSA = Southern Hemisphere South America, EURO = Europe, MIDE = Middle East, NHAF = Northern Hemisphere Africa, SHAF = Southern Hemisphere Africa, BOAS = Boreal Asia, SEAS = South East Asia, CEAS = Central Asia, EQAS = equatorial Asia, AUST = Australia.

compounds (NMVOC) and CH_4 [*Hooghiemstra et al*., 2011, 2012a, 2012b].

[32] We applied monthly mean CO emissions for four different categories: (1) anthropogenic (combustion of fossil and biofuels) emissions were taken from the Emissions Database for Global Atmospheric Research (EDGAR4.1, compiled for the year 2004) [*EDGAR Project Team*, 2010]. (2) The natural source consisted of direct emissions from plants and oceans [*Houweling et al*., 2008] and also the contribution of NMVOC-CO. (3) Optimized CH_4 mixing ratio fields [*Bergamaschi et al*., 2005] were used to take the CO production from oxidation of CH_4 into account. The last source (4) was BB, taken from GFED with the six different EF scenarios implemented. All sources except BB were kept the same in the different model runs. To make sure that atmospheric CO reached a quasi steady state mixing ratio for 2002–2007, we spun up for 2 years (starting at January 2000). With these sources and sinks defined, the CO budget closely resembles the one used in the a priori scenarios in the inverse study of *Hooghiemstra et al*. [2012b].

2.3. Observations of CO

[33] Surface flask observations of CO from the National Oceanic and Atmospheric Administration Earth System Research Laboratory (NOAA/ESRL) Cooperative Air Sampling Network (downloaded from ftp://ftp.cmdl.noaa.gov/ccg/co/flask/ in November 2011) were used for comparison with our transported bottom-up emissions. Currently, the NOAA/ESRL surface network consists of over 50 surface stations worldwide at which CO mixing ratios are weekly measured with very high analytical precision using flask samples [*Novelli et al*., 1998, 2003].

[34] Besides surface flask observations, we used CO total columns measurements from the Measurement of Pollution in the Troposphere (MOPITT) instrument onboard NASA's Terra satellite. The MOPITT version 4 (V4) product [*Deeter et al*., 2010] is based on the retrieval of CO in the thermal-infrared (TIR) at a wavelength of 4.7 mm [*Deeter*, 2003], and columns are mainly sensitive to CO in the free troposphere (altitudes of ~4–7 km). Although there is currently also a MOPITT version 5 (V5) product based on retrieved CO columns in both the TIR and the near-infrared, which is sensitive to CO in the boundary layer as well, we decided not to use this product in the current study since it is still considered "beta"-grade. However, a fully validated version of this V5 product will be very worthwhile to explore in the near future. Here we used the daily MOPITTV4 data product, gridded at a $1^\circ \times 1^\circ$ resolution, and applied the corresponding averaging kernel matrix to compare our modeled CO mixing ratios with individual measurements from MOPITT. We subsequently analyzed the results on a monthly basis over the years 2003–2006.

3. Results

[35] A description of the modeled bottom-up emission fields for the different EF scenarios is given in section 3.1. The modeled atmospheric CO mixing ratios are presented in section 3.2, and a comparison of our results, using both observed CO mixing ratios and recent inverse modeling results from other studies, is detailed in section 3.3.

3.1. Modeled CO Emission Fields

[36] Significant differences were found in mean annual CO emission estimates for the six EF scenarios, and across different regions in the world (Table 5 and Figure 2). Large variations occurred in the boreal regions, with on average higher annual CO emissions compared to GFED3 (currently using the GFED-A&M scenario) for boreal North America and boreal Asia. Of all EF scenarios, MCE-SEASON showed the largest increase for both regions; almost 40% more CO emissions were estimated in boreal North America for the 2002–2007 period, while in boreal Asia, the difference with GFED-A&M was even higher (~50%). The continent of Africa, contributing up to 43% of the global CO emissions over 2002–2007, showed lower CO emissions in all of our new scenarios; both Northern Hemisphere (NH) and Southern Hemisphere (SH) Africa decreased on average with ~3.5% annually. In SH South America, a range in emissions

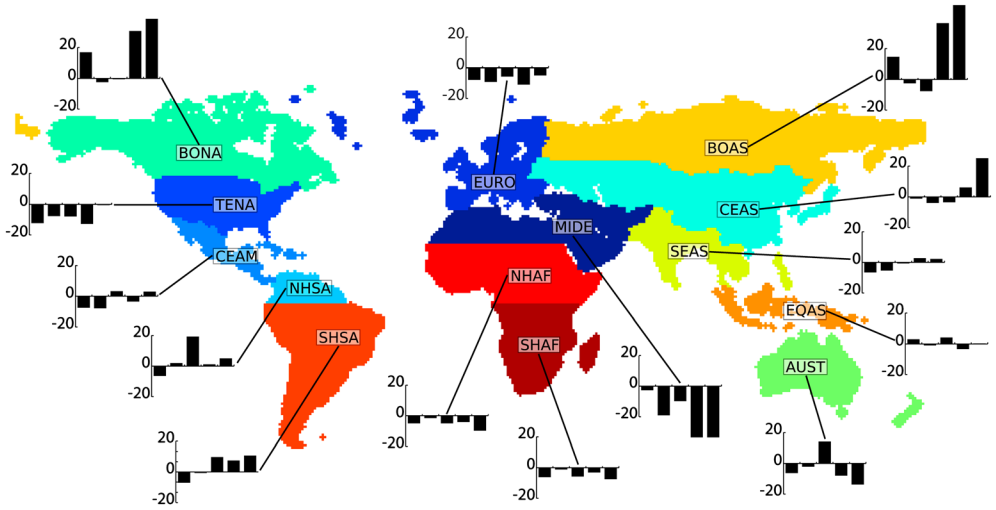

Figure 2. Global map of the 14 regions defined in this study and the differences (%) between mean annual CO emissions for the different EF scenarios and the standard GFED3 run (GFED-A&M). The bars (left to right) correspond to GFED-AKAGI, ENVI-A&M, ENVI-AKAGI, MCE-STATIC, MCE-SEASON. Abbreviations and emissions are given in Table 5.

of 58–69 Tg CO yr^{-1} was found for the different EF scenarios, and the mean (65 Tg CO) was more than 3% higher than GFED-A&M. A large relative difference (on average an ~17% decrease compared to GFED-A&M) was observed in the Middle East, but this region only contributes ~0.1% of global CO emissions.

[37] Spatial differences were also found within regions (Figure 3). Comparing ENVI-A&M, MCE-STATIC, and MCE-SEASON with the standard GFED3 run (GFED A&M), we observed higher CO emissions in tropical forested areas of NH Africa, SH Africa and SH South America, and lower values for savannas and grasslands in these regions.

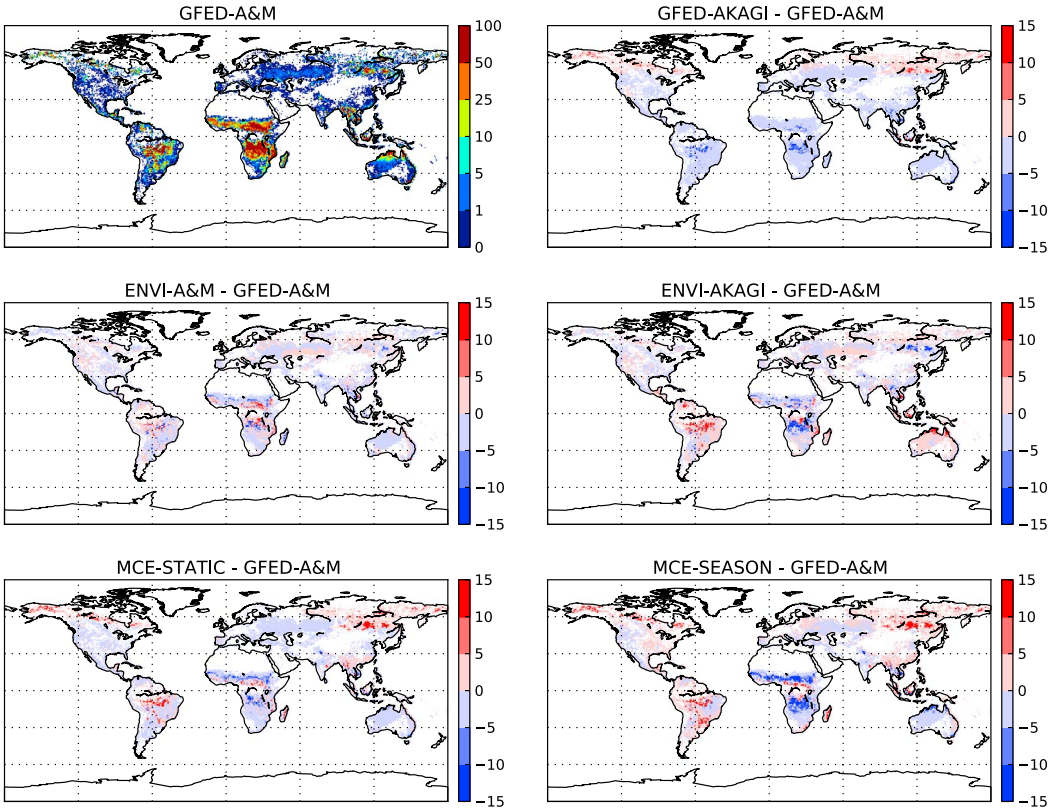

Figure 3. Mean emissions in Gg CO yr^{-1} for the (top left panel) GFED-A&M scenario, and the differences (Gg CO yr^{-1}) of GFED-AKAGI, ENVI-A&M, ENVI-AKAGI, MCE-STATIC, and MCE-SEASON with respect to GFED-A&M. All data are based on the 2002–2007 mean.

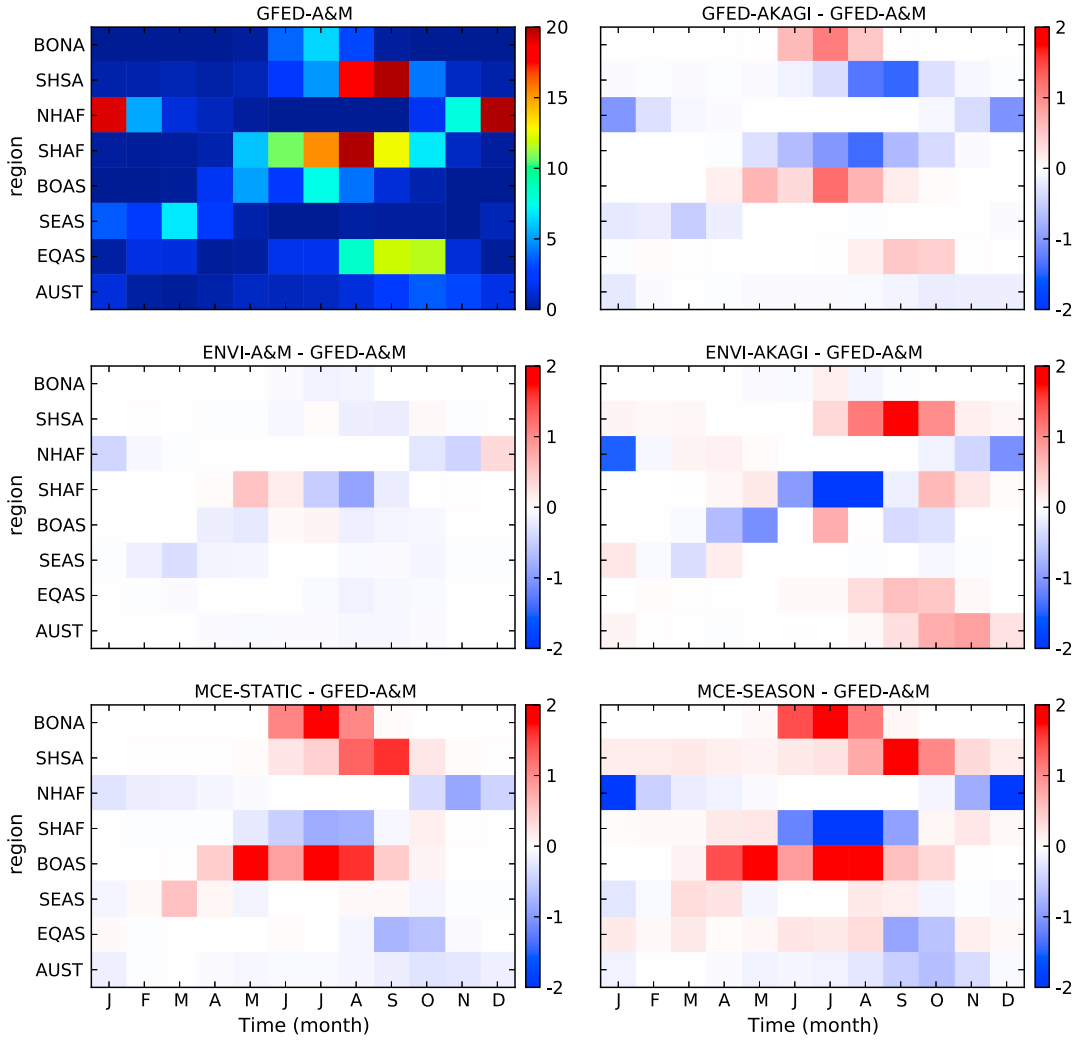

Figure 4. Mean seasonal cycle of CO emissions for the 2002–2007 period for eight important regions from a CO fire emissions perspective. In the upper left panel the GFED-A&M emissions are given in Tg CO month^{-1}, and the other panels show the differences (Tg CO month^{-1}) of GFED-AKAGI, ENVI-A&M, ENVI-AKAGI, MCE-STATIC, and MCE-SEASON with respect to GFED-A&M. See Table 5 for the list of region abbreviations.

Overall emissions for NH and SH Africa decreased (Table 5 and Figure 2) due to the relative large contribution of savanna and grassland fires. In general, we observed more spatial homogeneity within the boreal regions.

[38] Besides spatial differences, the EF scenarios also led to new and variable temporal patterns. In Figure 4, the mean seasonal cycle of CO emissions is shown for eight important fire regions. Peak fire months (PFM) for GFED-A&M (Figure 4, top left panel) usually occur in the local dry season in the tropics and the warmest months in the boreal region. For SH South-America and SH Africa, this was August and September, while in NH Africa, the months of December and January showed the highest fire emissions. In SH Africa, we observed higher emissions for the ENVI-AKAGI scenario in the early and late fire season, while CO emissions during the PFM were lower compared to GFED-A&M. Other scenarios, like MCE-STATIC and MCE-SEASON, showed more consistency during the season with lower emissions in SH Africa for all fire months. MCE-SEASON also estimated lower emissions during the PFM in equatorial Asia, but now, the other months showed higher emissions. For Boreal Asia and ENVI-AKAGI, this pattern was reversed, with higher emissions in the PFM and lower emissions during the rest of the year. Overall, the new EF scenarios led to substantially different spatial and temporal patterns from a bottom-up CO emission perspective.

3.2. Modeled Atmospheric CO Mixing Ratios

[39] Transport of bottom-up CO emission fields into the atmosphere with the TM5 model resulted in different atmospheric mixing ratios for the EF scenarios. The largest departure compared to the GFED standard runs were found for the MCE-SEASON scenario, shown in Figure 5. In the upper panel, the mean monthly CO mixing ratio enhancement due to BB is shown for GFED-A&M, clearly demonstrating the transport of CO to regions downwind of the fire source regions. In the lower panel, the difference between MCE-SEASON and GFED-A&M is shown. Most of the NH had higher CO burdens in MCE-SEASON, while the African continent showed lower mixing ratios than GFED-A&M. Typical

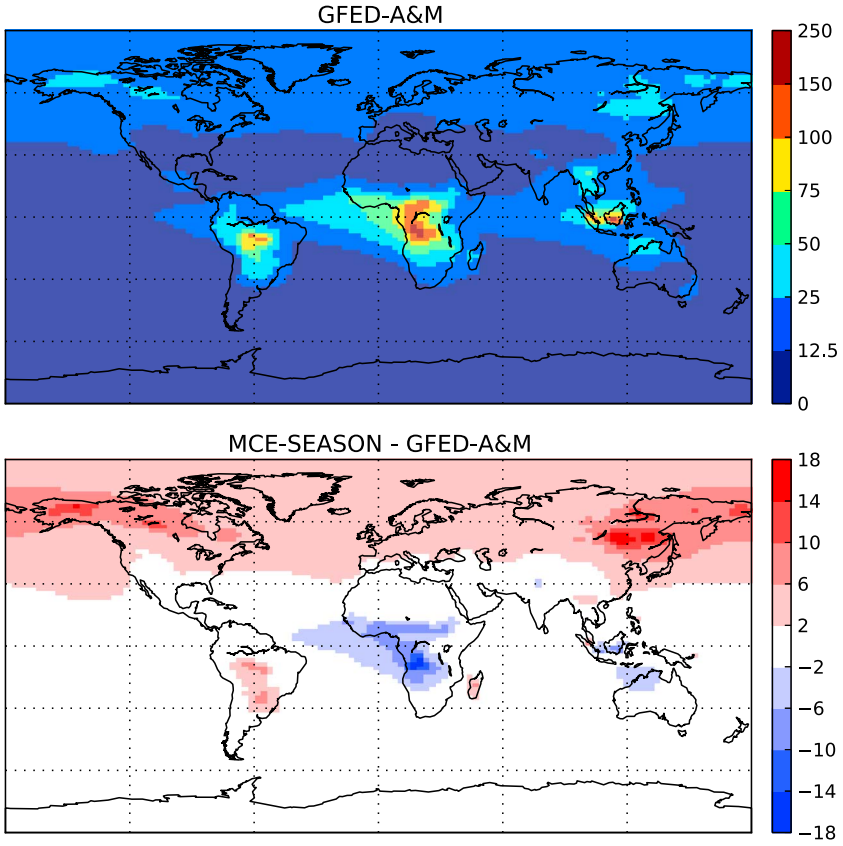

Figure 5. Mean CO mixing ratio enhancement due to biomass burning (ppb) for the (upper panel) GFED-A&M scenario, and the difference between (lower panel) MCE-SEASON and GFED-A&M. A monthly mean of the 2002–2007 period was used. CO mixing ratios were based on the seven lowest vertical layers, weighted by mass, corresponding to on average an atmospheric pressure of ~800 hPa on the top of layer 7.

differences found between both scenarios were 10–20 ppb, corresponding to ~35% of the GFED-A&M CO in the boreal areas and roughly ~10% in African fire hotspots.

[40] This difference in the NH and tropical mixing ratios was largest for MCE-SEASON, but also found in other scenarios as shown in Figure 6 where large-scale north-south gradients were plotted for the different EF scenarios. Instead of yearly averages, results are now shown for the months of June, July, August, and September only, since these months captured most of the fires in the boreal regions, southern Africa, Indonesia, and South America. Note that BB in northern Africa, clearly visible as a hot spot in Figure 5, is not very pronounced here since typical PFMs for that region are December and January. Moreover, the longitudinal averaging dampens the tropical signals because emissions occur only over the land regions that cover a smaller fraction of the tropics than the high northern latitudes. This averaging may also cancel large spatial differences across the tropical latitudes: e.g., MCE-SEASON estimated an increase of emissions above South-America (Figure 5, lower panel), but this difference is partly canceled by the lower emissions for the continent of Africa. The largest differences in mean latitudinal mixing ratios (~15 ppb) were found in the NH, where MCE-STATIC, MCE-SEASON, and GFED-AKAGI showed an increase compared to mixing ratios of GFED-A&M. Around the equator, GFED-A&M showed the highest mixing ratios, and in the SH, most scenarios agreed well.

[41] To investigate whether the new scenarios led to a temporal shift in peak CO mixing ratio, we plotted time series for three important fire regions in Figure 7. Large differences up to 30 ppb were observed in boreal North America during the months of June, July, and August, corresponding to an increase of ~40% compared to GFED3 estimates. In SH Africa, differences were the largest during the end of the dry season (corresponding to a decrease up to ~15% compared to GFED3 estimates), but we also found variations during the beginning of the dry season (May–July) for the years 2004 and 2005 (~15 ppb). In SH South America, the differences were not as pronounced, although deviations up to ~17 ppb were found during the end of the dry season in 2005. Overall, the temporal differences in the EF scenarios seem to be of the same magnitude as the spatial differences, with distinct month-to-month and even year-to-year variations in modeled CO mixing ratios. This suggests that in the interpretation of observed CO mixing ratios, the attribution of the CO growth rate to BB will depend again on the EF scenario assumed.

3.3. Comparison to Observed Atmospheric CO Mixing Ratios

[42] We used the NOAA surface stations that were most representative for important regions from a CO fire emission perspective. To choose these stations, we plotted the range of CO mixing ratios for the different EF scenarios

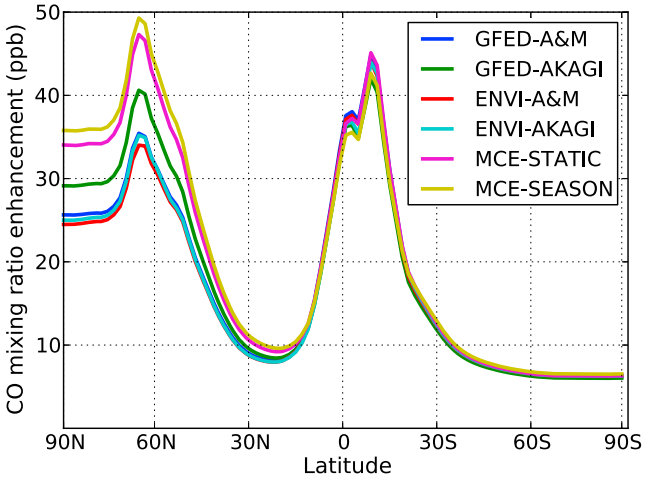

Figure 6. North-south CO gradient for six different EF scenarios, based on zonally averaged monthly biomass burning CO mixing ratios (ppb) for each 2° latitude bin. Values were based on the 2002–2007 mean for June–September. CO mixing ratios were based on the seven lowest vertical layers, weighted by mass, corresponding to on average an atmospheric pressure of ~800 hPa on the top of layer 7.

estimates in every TM5 model grid cell (Figure 8). In the upper panel—corresponding to the lower atmosphere (1000–800 hPa)—we observed the largest differences (up to 40 ppb) in Alaska, Siberia, Africa, and South America. Most stations are in the NH and few in the BB-dominated parts of the tropics and SH. The two stations that are most affected by BB with departures up to 20 pbb are Barrow Alaska (BRW) and Ascension Island (ASC). BRW was chosen to represent boreal fires of North America, and due to long-range transport, the station may capture CO from fires in boreal Asia as well. ASC is located in the Atlantic Ocean between Africa and South America. Since IAV in observed CO mixing ratios is relatively small [*Hooghiemstra et al.*, 2012b], the enhancement of CO over ASC was assumed to come mainly from emissions in Africa where the IAV in BB CO is less pronounced compared to South America [*Torres et al.*, 2010; *van der Werf et al.*, 2010].

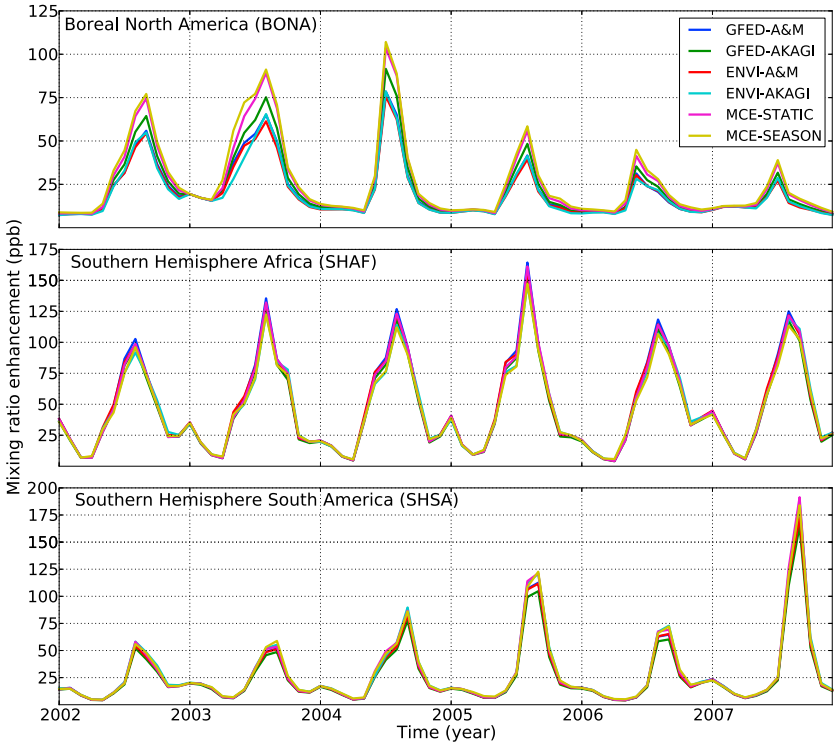

Figure 7. CO mixing ratio enhancement due to biomass burning (ppb) as modeled over BONA, SHAF, and SHSA for the 2002–2007 period. The CO mixing ratios shown here were based on the seven lowest vertical layers, weighted by mass, corresponding to on average an atmospheric pressure of ~800 hPa on the top of layer 7.

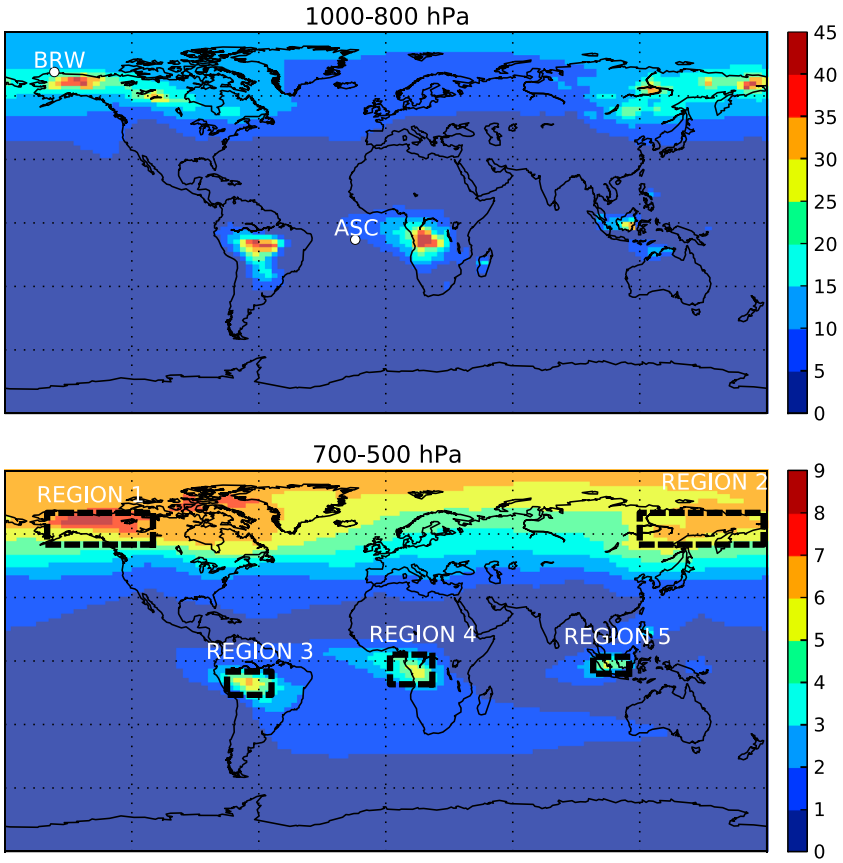

Figure 8. Range of CO mixing ratios (ppb) for the different EF scenarios. Results are shown for the 2002–2007 mean and for the months of June, July, August, and September only, since these months captured most of the fires in the boreal regions, southern Africa, Indonesia, and South America. In the upper panel the positioning of NOAA surface sites Barrow (BRW) and Ascension Island (ASC) is shown, and five regions used for the MOPITT comparison are spatially defined in the (dashed black lines) lower panel.

[43] In general, the modeled atmospheric mixing ratios followed the seasonal cycle of CO measurements well for BRW (Figure 9), although an underestimation of ~15–20 ppb existed similar to the findings of *Hooghiemstra et al.* [2012a]. This underestimation of modeled CO versus observations is a common bias in the boreal NH (as further discussed in section 4.2), and instead of interpreting this offset, we will therefore mostly focus on the temporal changes of the model and the measurements. The highest CO mixing ratios were observed from November to April, mainly due to anthropogenic sources. BB peaked in this region during May–August, and this is the period where we observed the largest differences between the EF-derived mixing ratios. Although GFED-AKAGI, MCE-STATIC, and MCE-SEASON showed higher CO mixing ratios than GFED-A&M and hence compared better with NOAA measurements, the differences between the EF scenarios were not large enough to conclude that the atmospheric observations of CO lend credibility to one EF scenario relative to the others: the temporal correlation coefficients (r) over the years 2002–2007 were in the 0.81–0.82 range for all EF scenarios. For ASC, the highest CO mixing ratios were observed from August to October, mainly due to BB in Africa and South America. Here the seasonal cycle was also captured reasonably well, although an underestimation of ~20 ppb existed mainly at the end of the dry season. Nevertheless, none of the EF scenarios improved the match with CO measurements from NOAA, suggesting that the atmospheric surface network, targeted mostly at relatively clean background conditions, is not well positioned to constrain BB plumes.

[44] In addition to the ground-based measurements, we used satellite observations of the MOPITT instrument to compare with our modeled mixing ratios above regions where BB played an important role. Five different areas were defined within the main BB regions in which relatively large differences between our modeled EF scenarios can be found, both at the surface and at heights at which the satellite measurements have the highest sensitivity (Figure 8, lower panel). Time series of the modeled CO mixing ratios and MOPITT observations for the different regions in the years 2003–2006 are shown in Figure 10. The largest differences between the EF scenarios were found for regions 1 and 2, located within respectively boreal NH and Asia. Although the seasonal cycle is captured relatively well, an underestimation of ~15 ppb compared to MOPITT existed. The temporal correlation coefficients over the years 2003–2006 indicated that MCE-SEASON performed best for regions 1 and 2 (Table 6): correlations of 0.91 with MOPITT were found, while ENVI-AKAGI was significantly lower (0.84 and 0.83 for regions 1 and 2, respectively).

[45] Located within the Brazilian Amazon, region 3 showed differences between the EF scenarios of up to

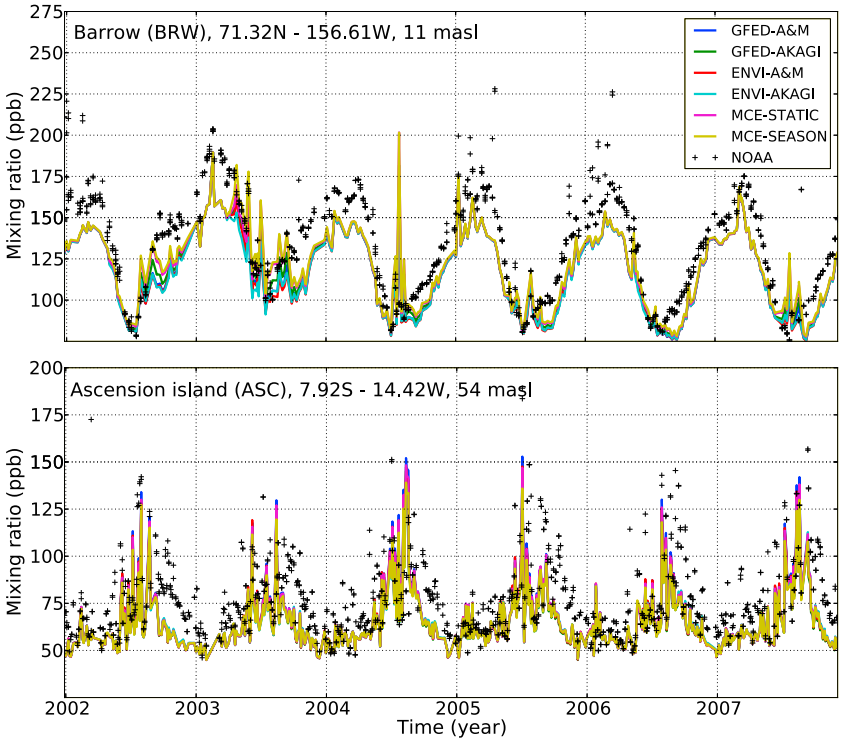

Figure 9. CO mixing ratios (ppb) of the different EF scenarios for NOAA stations Barrow (BRW) and Ascension Island (ASC) in the 2002–2007 period. Instead of biomass burning CO only, other sources and sinks—as described in section 2.2—were also included in modeled CO estimates. NOAA flask observations are shown in black crosses ("+").

~8 ppb during the fire season, while the underestimation of our modeled results compared to MOPITT is substantially larger (up to ~60 ppb in the year 2004). During the burning season, MOPITT measurements also peaked 1 month later than our modeled mixing ratios, similar to the findings of *Hooghiemstra et al*. [2012b] in this region. For all monthly CO observations over the 2003–2006 period, the highest correlations were found for ENVI-AKAGI (0.87). Similar to region 3, the maximum differences between the different EF scenarios in Africa (region 4) were ~8 ppb and in general MOPITT is about 15 ppb higher during the end of the burning. Moreover, our modeled mixing ratios peaked one to two months earlier than MOPITT observations. The correlation coefficients differed less pronouncedly and are in a range of 0.83–0.84 for all scenarios, indicating that none of the EF scenarios improved the temporal variations of the mixing ratios. Within region 5 (EQAS), the model output followed MOPITT estimates relatively well, although a slight underestimation was found for the months of August and September and an overestimation for January to March in the years 2003–2005. None of the EF scenarios clearly improved the temporal correlation (Table 6).

[46] As an alternative to both types of observations, we compared our results to recent inversion studies that often used atmospheric measurements in combination with satellite-derived CO columns to constrain the emissions. Our focus was on the year 2004, and we assumed that BB burning played a major role in the total emission estimates for the different regions of interest. In general, we found that most EF scenarios were in line with other inversion studies for boreal North America (Table 7): higher CO mixing ratios than GFED3 (using the GFED-A&M scenario) were suggested by all inversion studies and most of the EF scenarios, except for ENVI-A&M and ENVI-AKAGI. *Pison et al*. [2009] inverted emissions of CO, CH_4, and H_2 simultaneously over South America, using observations from NOAA and found lower CO emissions. GFED-AKAGI supported this finding. ENVI-A&M was in close agreement with GFED-A&M, while the other EF scenarios suggested more CO for this region. For Africa, most inverse modeling studies, except *Chevallier et al*. [2009] who performed a detailed analysis of African CO emissions using MOPITT data, suggested higher CO emissions than estimated by GFED3. However, three out of five EF scenarios showed a decrease in CO above Africa. For Australia the results were mixed as well: MCE-STATIC and MCE-SEASON showed a decrease in CO, and the same holds for the inverse modeling studies of *Hooghiemstra et al*. [2011] and *Pison et al*. [2009]. Using satellite data from two and three different instruments, respectively, both *Jones et al*. [2009] and *Kopacz et al*. [2010] suggested an increase of CO over the Australian continent. This was confirmed by ENVI-AKAGI only.

4. Discussion

4.1. Impact of Different EF Scenarios

[47] New EF emission fields impacted atmospheric concentrations globally, most pronounced over the African continent and boreal Alaska and Siberia. Focusing on the boreal regions, we showed CO mixing ratios varying up to 30 ppb in boreal North America in 2003 and 2004 (Figure 7), corresponding to an increase of ~40%

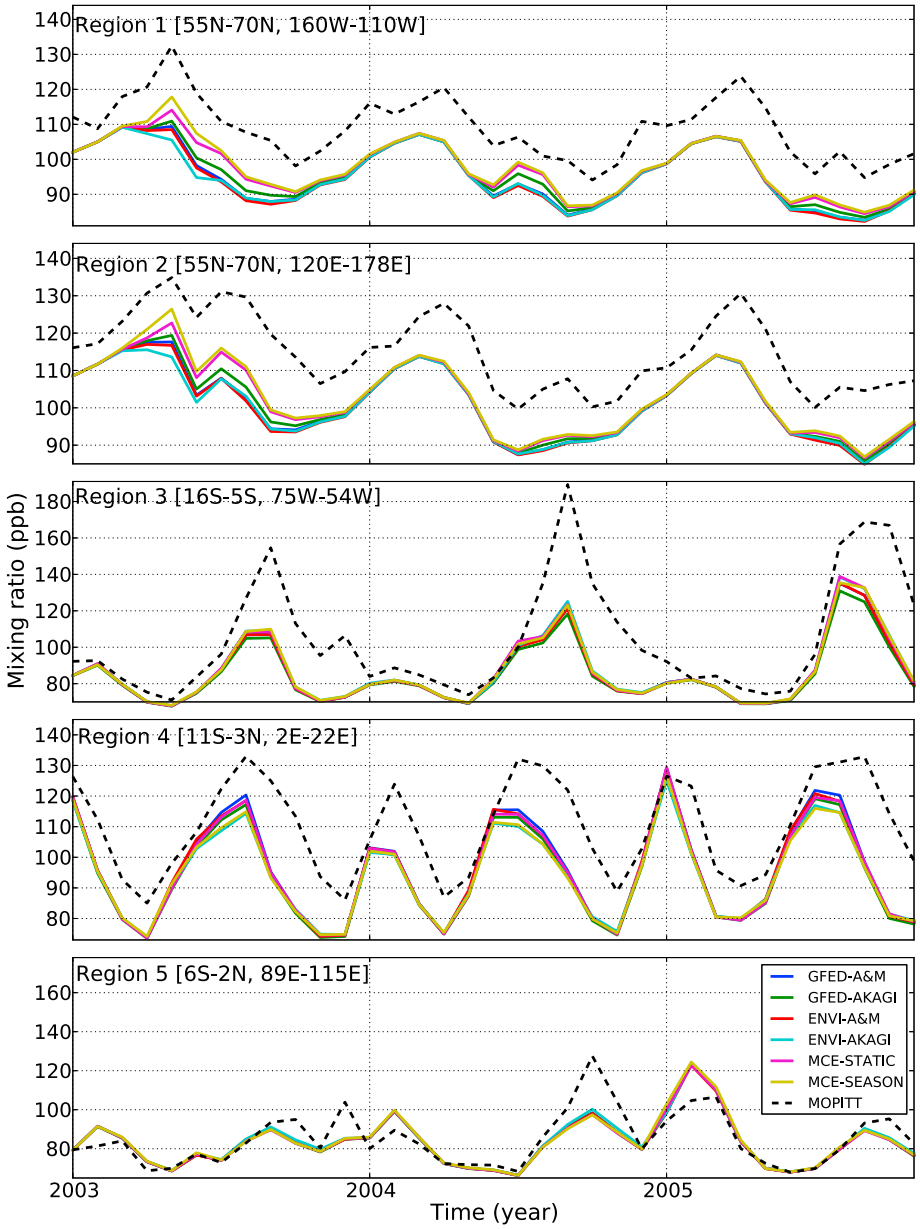

Figure 10. Average column CO mixing ratio (ppb) of the different EF scenarios over five regions for the 2003–2006 period. MOPITT satellite observations are shown in the dashed line. A spatial map of the locations defined can be found in the lower panel of Figure 8.

compared to GFED3 estimates. Both 2003 and 2004 were high fire years due to climatic conditions, and especially the fires that burned from June through September 2004 were the largest on record for Alaska [*Pfister et al.*, 2005]. The year 2003 saw high fire rates in Siberian forests as well due to a precipitation deficit during the period from August 2002 to May 2003 in the region [*Huang et al.*, 2009]. Thick haze caused by this fire event covered large parts of the boreal Asia for weeks, with smoke plumes travelling completely around the globe [*Bertschi and Jaffe*, 2005]. Like for boreal North America, the different EF scenarios showed an increase in CO mixing ratios compared to GFED3 for boreal Asia.

[48] The uncertainty in boreal fire emission estimates is large due to difficulties in modeling the consumption of the organic soil as the most important factor in governing emissions [*French et al.*, 2004]. The large ranges of EF-derived CO mixing ratios we found for boreal fires in 2003 and 2004 suggest that the contribution of EFs to this uncertainty is substantial and may therefore explain part of the underestimation of CO emission estimates by GFED that was found by *Yurganov et al.* [2011], *Huijnen et al.* [2012], and *Krol et al.* [2012] for the intensive Russian wildfires in 2010.

[49] The contribution of uncertainty in EFs to total uncertainty of the estimated CO budget will likely also impact assessment of other CO sources. Emissions of fossil fuel burning and the CO production from NMVOC emissions are often adapted in inverse modeling studies to match observations of CO (e.g., *Hooghiemstra et al.*, 2012a), and the different EF scenarios will likely lead to new results. A recent

Table 6. Temporal Correlation Coefficients (r) for Modeled CO Mixing Ratios Based on Six Different EF Scenarios and MOPITT Satellite Measurements[a]

Region	GFED-A&M	GFED-AKAGI	ENVI-A&M	ENVI-AKAGI	MCE-STATIC	MCE-SEASON
(1) BONA	0.87	0.89	0.87	0.84	0.90	*0.91*
(2) BOAS	0.85	0.87	0.84	0.83	*0.91*	*0.91*
(3) SHSA	0.84	0.84	0.85	*0.87*	0.84	0.86
(4) SHAF	*0.83*	0.82	0.81	0.82	*0.83*	0.81
(5) EQAS	0.79	0.79	0.80	*0.82*	0.78	0.77

[a]Correlations are based on monthly averages over the years 2003–2006. The best correlations per region for the six EF scenarios are shown in italic. Exact locations of the different regions can be found in the lower panel of Figure 8.

inversion study by *Hooghiemstra et al*. [2012b], based on GFED3 and thus the GFED-A&M scenario, required more BB emissions from South America to match MOPITT CO columns. Our simulations suggest that the use of any of the alternative EF scenarios would enhance the mismatch, since these EF scenarios produce even lower CO mixing ratios than GFED-A&M at heights where MOPITT is most sensitive (Figure 8, lower panel). On the other hand, choosing an alternative EF scenario would then also reduce CO mixing ratios in Africa and trigger a need for more BB emissions from this continent to compare well with MOPITT. Clearly, the impact of using different EF scenarios is likely to be substantial but complex.

4.2. Which EF Scenario?

[50] We consider MCE-SEASON as the most promising EF scenario of all, especially if we get a better handle on the fuel type partitioning in GFED and their corresponding MCE ranges. Assigning MCEs to specific fuel types allows us to better capture the variation within biomes: specifically accounting for the fraction of emissions stemming from litter and soil C may be useful in the boreal areas since the role of organic consumption is now taken into account. Within the savanna and grassland biome, the contribution of CWD could be important in separating woody from grassy vegetation. Moreover, the MCE scenario may be useful for the conversion to other trace gases and aerosols because they are directly linked to MCE. However, MCE-STATIC and MCE-SEASON are also the most experimental scenarios that need more validation.

[51] Focusing on EF scenarios where no temporal variability was included—MCE-STATIC, GFED-A&M, and GFED-AKAGI—the latter is the most useful for EFs of volatile compounds due to the focus on "fresh" plume measurements, and therefore allowing for a better representation of true initial conditions of a fire. Although this is not specifically important for CO, the uniform sampling protocol for EF measurements that was used by *Akagi et al*. [2011] may be an advantage over the use of EFs from *Andreae and Merlet* [2001], who took the mean of all EF measurements. Moreover, the spatial variation is larger in GFED-AKAGI than GFED-A&M due to the definition of three extra biomes, which may do justice to the differences between temperate and boreal fire characteristics.

[52] We are confident that EF scenarios that include a seasonal component (ENVI-A&M, ENVI-AKAGI, and MCE-SEASON) are more realistic than the ones that do not have this component, but we cannot assess whether the degree to which we model EF seasonality is right. In many BB regions, a strong seasonal cycle for different environmental parameters was found, with distinct dry seasons of low moisture and high temperatures toward the end of the dry season in, e.g., EQAS and SH South America. However, the exact relations between EFs and these environmental parameters are hard to constrain, both from a bottom-up and top-down perspective.

[53] As a first attempt to understand whether atmospheric observations of CO in the troposphere lend credibility to one or more EF scenarios relative to the others, we compared our results with NOAA station measurements. The range of

Table 7. Qualitative Comparison of Different Inversion Studies and the EF Scenario Mixing Ratios for Four Different Regions[a]

	Region			
Study	Boreal North America[b]	South America[c]	Africa[d]	Australia[e]
Hooghiemstra et al. [2011]	+	+	+	–
Kopacz et al. [2010]	+	+	+	+
Pison et al. [2009]	+	–	+	–
Jones et al. [2009]		+	+	+
Chevallier et al. [2009]			–	
GFED-AKAGI	+	–	–	=
ENVI-A&M	=	=	=	=
ENVI-AKAGI	=	+	–	+
MCE-STATIC	+	+	=	–
MCE-SEASON	+	+	–	–

[a]The "+" and "–" signs indicate that respectively higher and lower CO concentrations than GFED3 were found. The "=" sign indicates that results were in close agreement with GFED3 (within 5%).
[b]Mixing ratios above BOAS.
[c]Mixing ratios above South-America, so NHSA en SHSA combined.
[d]Mixing ratios above Africa, so NHAF en SHAF combined.
[e]Mixing ratios above AUST.

our EF derived mixing ratios for NOAA station locations was relatively small compared to BB regions in Africa, South America, and the boreal NH (Figure 8, upper panel), and although our modeled simulations captured the seasonal variation quite well for most of the stations, none of the EF scenarios improved the match with CO measurements. The mismatch between modeled and observed mixing ratios may be partly explained by the use of unoptimized emissions, as well as the existence of several limitations of the station data for evaluating BB emissions [*Bian et al*., 2007]. Especially in the boreal regions, an underestimation of CO by atmospheric transport models is common: *Mao et al*., 2013 argued that OH levels in the NH might be too high in many of the models and estimated that a decrease of OH concentrations drives an annual mean increase of model CO concentrations by 20–30 ppb. This increase of CO may explain a substantial part of the underestimation that we found for our modeled results and also largely corrects the bias for GEOS-CHem [*Alvarado et al*., 2010; *Fisher et al*., 2010; *Kopacz et al*., 2010] and several other model [*Shindell et al*., 2006] simulations in the boreal NH. Another potential source of bias are inaccurate emission estimates, and, e.g., *Hooghiemstra et al*. [2011] speculated that anthropogenic emissions in Asia were too low to reproduce the right CO concentrations for the NH.

[54] Since the different EF scenarios caused changes in CO mixing ratios up to 9 ppb at elevations where satellite sensors are sensitive (Figure 8, lower panel), we explored the use of CO column measurements derived from the MOPITT instrument. Similar to our comparison with NOAA stations, the observations from MOPITT indicated that the mismatch between modeled and observed was substantially larger than the differences found between the EF scenarios, with, in general, a negative bias (ratio model output to MOPITT) for most of the regions (Figure 10). However, temporal correlations over the 2003–2006 period significantly improved for specific EF scenarios (Table 6): in the boreal regions, the highest correlations were found for both MCE-STATIC and MCE-SEASON, indicating that the definition of fuel type–specific EFs might be important for fire emission modeling within these regions. Over South America and Indonesia, the influence of EF seasonality seemed to be important since the highest correlations (0.87 and 0.82, respectively) were found for ENVI-AKAGI, the scenario that is driven by several environmental data sets. Comparing GFED-A&M and GFED-AKAGI, the two EF scenarios that used biome-averaged EF and in which no seasonality is included, we found that the scenario relying on the EF database of *Akagi et al*. [2011] showed the best performance compared to MOPITT data in most of the regions. The uniform sampling protocol used for EF measurements and the definition of three extra EF specific biomes may have caused this better fit.

[55] As an alternative approach to rate the different EF scenarios, a quantitative comparison with recent inverse modeling studies for the year 2004 was made. This exercise yielded conflicting results and could not identify one EF scenario as superior over the others. Partly, this could be because these studies focused on slightly different regions and time periods, but it is also likely that the observations (both satellite derived and sampled from the atmosphere) simply do not yet have the resolving power to distinguish one EF scenario from another well enough. An interesting new opportunity for such inverse modeling studies is offered through our MCE approach: instead of optimizing BB emissions directly, the inverse models could try to optimize the MCEs of each fuel type, and thereby extrapolate "local" information from measurements directly influenced by burning to larger areas of the globe.

4.3. Sources of Uncertainty

[56] Our work included many steps, each bearing uncertainties that are not always easily quantified. Below we qualitatively discuss the uncertainties related to the different EF scenarios. Focusing on the different scenarios we developed, both GFED-A&M and GFED-AKAGI used biome-averaged EFs that did not change through the season. In addition to the assumption that EFs do not change from 1 month to the other, the definition of a specific biome carries uncertainty: *Andreae and Merlet* [2001] compiled EF measurements for four different biomes; extratropical forest, tropical forest, savanna and grassland, and agricultural area. The extratropical forest biome covers both boreal and temporal forests, although EFs for both vegetation types are likely to differ. *Akagi et al*. [2011] defined two additional biomes and separated the boreal and temperate forests. Using the same EF for specific biomes all over the world introduces another uncertainty: e.g., savanna fires in Australia are assumed to burn with the same CO EF as African savannas or Cerrado fires in Brazil. The same is true for tropical forest fires in Brazil, Mexico, and Africa, or boreal forest fires in Alaska and Siberia.

[57] In both ENVI-A&M and ENVI-AKAGI, a temporal variability in CO EFs was added, based on the assumption that the condition of the regional environment would correlate with the regional CO EF. Since our work is based on coarse $0.5^\circ \times 0.5^\circ$ data sets and landscapes are often heterogeneous, the average environment for a large area will not correlate perfectly with the few available point measurements. Although reasonable correlations were found for specific case studies, the multivariate relations based on all the full suite of EF measurements of *Andreae and Merlet* [2001] and *Akagi et al*. [2011] were lower and explained ~28% of the variability for CO. This may be partly due to uncertainties in the EF measurements used and the different environmental data sets [*van Leeuwen and van der Werf*, 2011]. Further, we noticed that the fire process is very complex, and the exact relationships between different burning conditions and the emissions are not well understood yet. Besides ambient conditions, other factors, like fuel density, fuel spacing, and an efficient heat transfer, play a large and complex role in the emissions, but this is very difficult to take into account in a coarse resolution model like GFED.

[58] For MCE-STATIC and MCE-SEASON, we used predefined MCEs for seven different fuel types, which is a novel way in the GFED modeling framework to calculate trace gas emissions. In addition to the assumption that the partitioning of different fuel types in the biogeochemical GFED-CASA model is correct, data on how MCEs of specific fuel types evolve over time are limited, and in some cases, nonexisting. Because of this lack of data, the definition of specific MCEs for both scenarios is for some fuel types that are highly experimental and based on our own judgment. Although we acknowledge that a change in the

fuel type–specific MCEs will impact emission estimates substantially, we feel that this scenario offers an interesting alternative to the other scenarios, and it will be explored further in future versions of GFED.

[59] Finally, even a "perfect" EF scenario depends on the calculation of bottom-up C emissions. In the GFED modeling framework, C emission estimates for BB are basically based on three quantities—burned area, fuel loads, and combustion completeness—all bearing their own uncertainties. The main uncertainties for these quantities are described in section 1, and for a more extensive description, we refer to *van der Werf et al*. [2006, 2010]. In general, uncertainties in global fire C emissions are reducing due to improvement of the quality of the input data sets [*van der Werf et al*., 2010], but are still estimated to about 20% at an annual scale. Uncertainties increase when smaller regions or shorter time windows are considered. To improve our understanding of the impact of seasonal and temporal variable EFs on total CO emissions, we need to get a better handle on the uncertainties of the different quantities involved in the modeling framework. Sensitive experiments as conducted by *Bian et al*. [2007] provide useful information regarding these uncertainties.

[60] Overall, our new scenarios provided a physically plausible way forward, but addressing the uncertainty proved difficult. More ground measurements are needed to increase our knowledge on the partitioning of biomass burned in different trace gases and aerosols, with a focus on understanding temporal variations and the different drivers that affect EF variability. Following the work of *Chen et al*. [2010], an important step forward could be the setup of several lab experiments to test the role of different environmental parameters—like, e.g., soil moisture and temperature—on EFs for different vegetation types.

5. Conclusions

[61] We developed new biomass burning emission factor (EF) scenarios for use in large-scale fire emission assessments, including a component of spatial and temporal variability. These new scenarios were used to construct CO emission fields, which we transported into the atmosphere with the TM5 chemistry transport model.

[62] Our work demonstrated the potential importance of accounting for spatial and temporal variations of EFs in fire emission modeling, and new EF fields impacted emission estimates of CO considerably. Most of the EF scenarios suggested an increase of CO emission estimates in boreal regions compared to the GFED standard run with differences up to 50% for total CO emissions for the 2002–2007 period. Over the continent of Africa, lower values were estimated, with on average a total annual decrease of ~3.5%. The new emission fields also caused changes in corresponding atmospheric mixing ratios of CO. A range of 30 ppb over boreal North America was found between the various EF scenarios during the burning season, and for both Africa and South America, values varied over 15 ppb depending on the EF scenario. Our findings suggest that the choice of EF scenario can alter the interpretation of observed mixing ratios, such as in inverse studies, substantially.

[63] We consider the EF scenarios that included temporal variations more physically sound than static EF scenarios due to the substantial seasonality of different environmental parameters found in most biomass burning regions. However, exact relations between these parameters and the EFs cannot be extracted from the current body of literature. The Modified Combustion Efficiency (MCE), a measure for the relative amount of flaming and smoldering combustion during a fire, was used in a promising new method that is based on the definition of fuel type–specific MCEs.

[64] Unfortunately, remote surface observations of CO in the troposphere and recent inverse modeling studies did not lend credibility to one or more EF scenarios relative to the others. A satellite-based comparison indicated that the choice of EF scenario might be region-specific: in the boreal biomass burning regions, the fuel type–specific approach performed better, while including EF seasonality through environmental variables played a more important role in South America and Indonesia. The use of higher spatial and temporal resolution data could be an important next step in validating these regional differences between the various EF scenarios.

[65] **Acknowledgments.** We greatly appreciate the efforts of the emission factor community to conduct the measurements, and thank Bob Yokelson for useful discussions and comments. We kindly acknowledge Dr. P. Novelli for the use of the CO observations from the Cooperative Air Sampling Program coordinated by NOAA ESRL and thank M. Deeter for his contributions to the MOPITT CO data. Thijs van Leeuwen was supported by the Dutch User Support Programme from the Netherlands organization for scientific research (NWO) under program number GO/AO-11. Wouter Peters was partially supported by an NWO VIDI grant (864.08.012) and Guido van der Werf received support from the European Research Council (ERC) grant number 280061.

References

Akagi, S. K., R. J. Yokelson, C. Wiedinmyer, M. J. Alvarado, J. S. Reid, T. Karl, J. D. Crounse, and P. O. Wennberg (2011), Emission factors for open and domestic biomass burning for use in atmospheric models, *Atmos. Chem. Phys.*, *11*(9), 4039–4072, doi:10.5194/acp-11-4039-2011.

Alvarado, M. J., et al. (2010), Nitrogen oxides and PAN in plumes from boreal fires during ARCTAS-B and their impact on ozone: An integrated analysis of aircraft and satellite observations, *Atmos. Chem. Phys.*, *10*(20), 9739–9760, doi:10.5194/acp-10-9739-2010.

Andreae, M. O., and P. Merlet (2001), Emission of trace gases and aerosols from biomass burning, *Global Biogeochem. Cycles*, *15*(4), 955–966, doi:10.1029/2000GB001382.

Arellano, A. F., P. S. Kasibhatla, L. Giglio, G. R. Van Der Werf, J. T. Randerson, and G. J. Collatz (2006), Time-dependent inversion estimates of global biomass-burning CO emissions using Measurement of Pollution in the Troposphere (MOPITT) measurements, *J. Geophys. Res.*, *111*, D09303, doi:10.1029/2005JD006613.

Bergamaschi, P., M. Krol, F. Dentener, A. Vermeulen, F. Meinhardt, R. Graul, M. Ramonet, W. Peters, and E. J. Dlugokencky (2005), Inverse modelling of national and European CH4 emissions using the atmospheric zoom model TM5, *Atmos. Chem. Phys.*, *5*, 2431–2460.

Bertschi, I. T., and D. A. Jaffe (2005), Long-range transport of ozone, carbon monoxide, and aerosols to the NE Pacific troposphere during the summer of 2003: Observations of smoke plumes from Asian boreal fires, *J. Geophys. Res.*, *110*, D05303, doi:10.1029/2004JD005135.

Bertschi, I., R. J. Yokelson, D. E. Ward, R. E. Babbitt, R. A. Susott, J. G. Goode, and W. M. Hao (2003), Trace gas and particle emissions from fires in large diameter and belowground biomass fuels, *J. Geophys. Res.*, *108*(D13), 8472, doi:10.1029/2002JD002100.

Bian, H., M. Chin, S. R. Kawa, B. Duncan, A. Arellano, and P. Kasibhatla (2007), Sensitivity of global CO simulations to uncertainties in biomass burning sources, *J. Geophys. Res.*, *112*, D23308, doi:10.1029/2006JD008376.

Bowman, D. M. J. S., et al. (2009), Fire in the Earth System, *Science*, *324*(5926), 481–484, doi:10.1126/science.1163886.

Burling, I. R., et al. (2010), Laboratory measurements of trace gas emissions from biomass burning of fuel types from the southeastern and southwestern United States, *Atmos. Chem. Phys.*, *10*(22), 11115–11130, doi:10.5194/acp-10-11115-2010.

Burling, I. R., R. J. Yokelson, S. K. Akagi, S. P. Urbanski, C. E. Wold, D. W. T. Griffith, T. J. Johnson, J. Reardon, and D. R. Weise (2011),

Airborne and ground-based measurements of the trace gases and particles emitted by prescribed fires in the United States, *Atmos. Chem. Phys.*, *11*(23), 12197–12216, doi:10.5194/acp-11-12197-2011.

Chen, L. W. A., P. Verburg, A. Shackelford, D. Zhu, R. Susfalk, J. C. Chow, and J. G. Watson (2010), Moisture effects on carbon and nitrogen emission from burning of wildland biomass, *Atmos. Chem. Phys.*, *10*(14), 6617–6625, doi:10.5194/acp-10-6617-2010.

Chevallier, F., A. Fortems, P. Bousquet, I. Pison, S. Szopa, M. Devaux, and D. A. Hauglustaine (2009), African CO emissions between years 2000 and 2006 as estimated from MOPITT observations, *Biogeosciences*, *6*(1), 103–111.

Christian, T. J., B. Kleiss, R. J. Yokelson, R. Holzinger, P. J. Crutzen, W. M. Hao, B. H. Saharjo, and D. E. Ward (2003), Comprehensive laboratory measurements of biomass-burning emissions: 1. Emissions from Indonesian, African, and other fuels, *J. Geophys. Res.*, *108*(D23), 4719, doi:10.1029/2003JD003704.

Crutzen, P. J., and M. O. Andreae (1990), Biomass burning in the tropics—Impact on atmospheric chemistry and biogeochemical cycles, *Science*, *250*(4988), 1669–1678.

Deeter, M. N. (2003), Operational carbon monoxide retrieval algorithm and selected results for the MOPITT instrument, *J. Geophys. Res.*, *108*(D14), 4399, doi:10.1029/2002JD003186.

Deeter, M. N., et al. (2010), The MOPITT version 4 CO product: Algorithm enhancements, validation, and long-term stability, *J. Geophys. Res.*, *115*, D07306, doi:10.1029/2009JD013005.

Delmas, R., J. P. Lacaux, and D. Brocard (1995), Determination of biomass burning emission factors: Methods and results, vol. 38, pp. 181–204.

EDGAR Project Team (2010), Emission Database for Global Atmospheric Research (EDGAR), release version 4.1, http://edgar.jrc.ec.europa.eu, Eur. Comm. Joint Res. Cent., Ispra, Italy.

Edwards, D. P., et al. (2004), Observations of carbon monoxide and aerosols from the Terra satellite: Northern Hemisphere variability, *J. Geophys. Res.*, *109*, D24202, doi:10.1029/2004JD004727.

Ferek, R. J., J. S. Reid, P. V. Hobbs, D. R. Blake, and C. Liousse (1998), Emission factors of hydrocarbons, halocarbons, trace gases and particles from biomass burning in Brazil, *J. Geophys. Res.*, *103*(D24), 32107–32118, doi:10.1029/98JD00692.

Fisher, J. A., D. J. Jacob, M. T. Purdy, M. Kopacz, P. Le Sager, C. Carouge, C. D. Holmes, R. M. Yantosca, R. L. Batchelor, and K. Strong (2010), Source attribution and interannual variability of Arctic pollution in spring constrained by aircraft (ARCTAS, ARCPAC) and satellite (AIRS) observations of carbon monoxide, *Atmos. Chem. Phys.*, *10*(3), 977–996.

French, N., P. Goovaerts, and E. S. Kasischke (2004), Uncertainty in estimating carbon emissions from boreal forest fires, *J. Geophys. Res.*, *109*, D14S08, doi:10.1029/2003JD003635.

Giglio, L., T. Loboda, D. P. Roy, B. Quayle, and C. O. Justice (2009), An active-fire based burned area mapping algorithm for the MODIS sensor, *Remote Sens. Environ.*, *113*(2), 408–420, doi:10.1016/j.rse.2008.10.006.

Giglio, L., J. T. Randerson, G. R. Van Der Werf, P. S. Kasibhatla, G. J. Collatz, D. C. Morton, and R. S. DeFries (2010), Assessing variability and long-term trends in burned area by merging multiple satellite fire products, *Biogeosciences*, *7*(3), 1171–1186.

Gloudemans, A. M. S., M. C. Krol, J. F. Meirink, A. T. J. De Laat, G. R. Van Der Werf, H. Schrijver, M. M. P. Van Den Broek, and I. Aben (2006), Evidence for long-range transport of carbon monoxide in the Southern Hemisphere from SCIAMACHY observations, *Geophys. Res. Lett.*, *33*, L16807, doi:10.1029/2006GL026804.

Goode, J. G., R. J. Yokelson, R. A. Susott, and D. E. Ward (1999), Trace gas emissions from laboratory biomass fires measured by open-path Fourier transform infrared spectroscopy: Fires in grass and surface fuels, *J. Geophys. Res.*, *104*(D17), 21237–21245, doi:10.1029/1999JD900360.

Hely, C., S. Alleaume, R. J. Swap, H. H. Shugart, and C. O. Justice (2003), SAFARI-2000 characterization of fuels, fire behavior, combustion completeness, and emissions from experimental burns in infertile grass savannas in western Zambia, *J. Arid Environ.*, *54*(2), 381–394, doi:10.1006/jare.2002.1097.

Hoelzemann, J. J., M. G. Schultz, and G. P. Brasseur (2004), Global Wildland Fire Emission Model (GWEM): Evaluating the use of global area burnt satellite data, *J. Geophys. Res.*, *109*, D14S04, doi:10.1029/2003JD003666.

Hoffa, E. A., D. E. Ward, W. M. Hao, R. A. Susott, and R. H. Wakimoto (1999), Seasonality of carbon emissions from biomass burning in a Zambian savanna, *J. Geophys. Res.*, *104*(D11), 13841–13853, doi:10.1029/1999JD900091.

Hooghiemstra, P. B., M. C. Krol, J. F. Meirink, P. Bergamaschi, G. R. Van Der Werf, P. C. Novelli, I. Aben, and T. Röckmann (2011), Optimizing global CO emission estimates using a four-dimensional variational data assimilation system and surface network observations, *Atmos. Chem. Phys.*, *11*(10), 4705–4723, doi:10.5194/acp-11-4705-2011.

Hooghiemstra, P. B., M. C. Krol, P. Bergamaschi, A. T. J. De Laat, G. R. Van Der Werf, P. C. Novelli, M. N. Deeter, I. Aben, and T. Röckmann (2012a), Comparing optimized CO emission estimates using MOPITT or NOAA surface network observations, *J. Geophys. Res.*, *117*, D06309, doi:10.1029/2011JD017043.

Hooghiemstra, P. B., M. C. Krol, T. T. Van Leeuwen, G. R. Van Der Werf, P. C. Novelli, M. N. Deeter, I. Aben, and T. Röckmann (2012b), Interannual variability of carbon monoxide emission estimates over South America from 2006 to 2010, *J. Geophys. Res.*, *117*, D15308, doi:10.1029/2012JD017758.

Houweling, S., G. R. Van Der Werf, K. K. Goldewijk, T. Roeckmann, and I. Aben (2008), Early anthropogenic CH4 emissions and the variation of CH4 and (CH4)-C-13 over the last millennium, *Global Biogeochem. Cycles*, *22*, GB1002, doi:10.1029/2007GB002961.

Huang, S., F. Siegert, J. G. Goldammer, and A. I. Sukhinin (2009), Satellite-derived 2003 wildfires in southern Siberia and their potential influence on carbon sequestration, *Int. J. Remote Sens.*, *30*(6), 1479–1492, doi:10.1080/01431160802541549.

Huijnen, V., et al. (2010), The global chemistry transport model TM5: Description and evaluation of the tropospheric chemistry version 3.0, *Geosci. Model Dev.*, *3*(2), 445–473, doi:10.5194/gmd-3-445-2010.

Huijnen, V., et al. (2012), Hindcast experiments of tropospheric composition during the summer 2010 fires over western Russia, *Atmos. Chem. Phys.*, *12*(9), 4341–4364, doi:10.5194/acp-12-4341-2012.

Ito, A., and J. E. Penner (2004), Global estimates of biomass burning emissions based on satellite imagery for the year 2000, *J. Geophys. Res.*, *109*, D14S05, doi:10.1029/2003JD004423.

Ito, A., and J. E. Penner (2005), Estimates of CO emissions from open biomass burning in southern Africa for the year 2000, *J. Geophys. Res.*, *110*, D19306, doi:10.1029/2004JD005347.

Janhaell, S., M. O. Andreae, and U. Poeschl (2010), Biomass burning aerosol emissions from vegetation fires: Particle number and mass emission factors and size distributions, *Atmos. Chem. Phys.*, *10*(3), 1427–1439.

Johnston, F. H., S. B. Henderson, Y. Chen, J. T. Randerson, M. Marlier, R. S. DeFries, P. Kinney, D. M. J. S. Bowman, and M. Brauer (2012), Estimated global mortality attributable to smoke from landscape fires, *Environ. Health Perspect.*, *120*(5), 695–701, doi:10.1289/ehp.1104422.

Jones, D. B. A., K. W. Bowman, J. A. Logan, C. L. Heald, J. Liu, M. Luo, J. Worden, and J. Drummond (2009), The zonal structure of tropical O-3 and CO as observed by the Tropospheric Emission Spectrometer in November 2004—Part 1: Inverse modeling of CO emissions, *Atmos. Chem. Phys*, *9*(11), 3547–3562.

Koch, D., T. C. Bond, D. Streets, N. Unger, and G. R. van der Werf (2007), Global impacts of aerosols from particular source regions and sectors, *J. Geophys. Res.*, *112*, D02205, doi:10.1029/2005JD007024.

Kopacz, M., et al. (2010), Global estimates of CO sources with high resolution by adjoint inversion of multiple satellite datasets (MOPITT, AIRS, SCIAMACHY, TES), *Atmos. Chem. Phys.*, *10*(3), 855–876.

Korontzi, S. (2005), Seasonal patterns in biomass burning emissions from southern African vegetation fires for the year 2000, *Global Change Biol.*, *11*(10), 1680–1700, doi:10.1111/j.1365-2486.2005.01024.x.

Korontzi, S., C. O. Justice, and R. J. Scholes (2003a), Influence of timing and spatial extent of savanna fires in southern Africa on atmospheric emissions, *J. Arid Environ*, *54*, 395–404, doi:10.1006/jare.2002.1098.

Korontzi, S., D. E. Ward, R. A. Susott, R. J. Yokelson, C. O. Justice, P. V. Hobbs, E. Smithwick, and W. M. Hao (2003b), Seasonal variation and ecosystem dependence of emission factors for selected trace gases and PM2.5 for southern African savanna fires, *J. Geophys. Res.*, *108*(D24), 4758, doi:10.1029/2003JD003730.

Korontzi, S., D. P. Roy, C. O. Justice, and D. E. Ward (2004), Modeling and sensitivity analysis of fire emissions in southern Africa during SAFARI 2000, *Remote Sens. Environ.*, *92*, 255–275, doi:10.1016/j.rse.2004.06.010.

Krol, M., S. Houweling, B. Bregman, M. Van Den Broek, A. Segers, P. Van Velthoven, W. Peters, F. Dentener, and P. Bergamaschi (2005), The two-way nested global chemistry-transport zoom model TM5: Algorithm and applications, *Atmos. Chem. Phys.*, *5*, 417–432.

Krol, M., et al. (2012), How much CO was emitted by the 2010 fires around Moscow? *Atmos. Chem. Phys Discuss.*, *12*(11), 28705–28731, doi:10.5194/acpd-12-28705-2012. [online] Available from: http://atmos-chem-phys-discuss.net/12/28705/2012/acpd-12-28705-2012.pdf

Langenfelds, R., R. Francey, B. Pak, L. Steele, J. Lloyd, C. Trudinger, and C. Allison (2002), Interannual growth rate variations of atmospheric CO2 and its delta C-13, H-2, CH4, and CO between 1992 and 1999 linked to biomass burning, *Global Biogeochem. Cycles*, *16*(3), 1048, doi:10.1029/2001GB001466.

van Leeuwen, T. T., and G. R. Van Der Werf (2011), Spatial and temporal variability in the ratio of trace gases emitted from biomass burning, *Atmos. Chem. Phys.*, *11*(8), 3611–3629, doi:10.5194/acp-11-3611-2011.

Mao, J., S. Fan, D. J. Jacob, and K. R. Travis (2013), Radical loss in the atmosphere from Cu-Fe redox coupling in aerosols, *Atmos. Chem. Phys.*, *13*(2), 509–519, doi:10.5194/acp-13-509-2013.

McMeeking, G. R., et al. (2009), Emissions of trace gases and aerosols during the open combustion of biomass in the laboratory, *J. Geophys. Res.*, *114*, D19210, doi:10.1029/2009JD011836.

Meyer, C. P., G. D. Cook, F. Reisen, T. E. L. Smith, M. Tattaris, J. Russell-Smith, S. W. Maier, C. P. Yates, and M. J. Wooster (2012), Direct measurements of the seasonality of emission factors from savanna fires in northern Australia, *J. Geophys. Res.*, *117*, D20305, doi:10.1029/2012JD017671.

Naeher, L. P., M. Brauer, M. Lipsett, J. T. Zelikoff, C. D. Simpson, J. Q. Koenig, and K. R. Smith (2007), Woodsmoke health effects: A review, *Inhalation Toxicol.*, *19*(1), 67–106, doi:10.1080/08958370600985875.

Novelli, P. C., K. A. Masarie, and P. M. Lang (1998), Distributions and recent changes of carbon monoxide in the lower troposphere, *J. Geophys. Res.*, *103*(D15), 19015–19033, doi:10.1029/98JD01366.

Novelli, P. C., K. A. Masarie, P. M. Lang, B. D. Hall, R. C. Myers, and J. W. Elkins (2003), Reanalysis of tropospheric CO trends: Effects of the 1997–1998 wildfires, *J. Geophys. Res.*, *108*(D15), 4464, doi:10.1029/2002JD003031.

Pfister, G., P. G. Hess, L. K. Emmons, J. F. Lamarque, C. Wiedinmyer, D. P. Edwards, G. Pétron, J. C. Gille, and G. W. Sachse (2005), Quantifying CO emissions from the 2004 Alaskan wildfires using MOPITT CO data, *Geophys. Res. Lett.*, *32*, L11809, doi:10.1029/2005GL022995.

Pison, I., P. Bousquet, F. Chevallier, S. Szopa, and D. Hauglustaine (2009), Multi-species inversion of CH4, CO and H-2 emissions from surface measurements, *Atmos. Chem. Phys.*, *9*(14), 5281–5297.

Randerson, J. T., Y. Chen, G. R. Van Der Werf, B. M. Rogers, and D. C. Morton (2012), Global burned area and biomass burning emissions from small fires, *J. Geophys. Res.*, *117*, G04012, doi:10.1029/2012JG002128.

Roy, D. P., and L. Boschetti (2009), Southern Africa Validation of the MODIS, L3JRC, and GlobCarbon Burned-Area Products, *IEEE Trans. Geosci. Remote Sens.*, *47*(4), 1032–1044, doi:10.1109/TGRS.2008.2009000.

Roy, D. P., L. Boschetti, C. O. Justice, and J. Ju (2008), The collection 5 MODIS burned area product—Global evaluation by comparison with the MODIS active fire product, *Remote Sens. Environ.*, *112*(9), 3690–3707, doi:10.1016/j.rse.2008.05.013.

Shindell, D. T., et al. (2006), Multimodel simulations of carbon monoxide: Comparison with observations and projected near-future changes, *J. Geophys. Res.*, *111*, D19306, doi:10.1029/2006JD007100.

Sitch, S., P. M. Cox, W. J. Collins, and C. Huntingford (2007), Indirect radiative forcing of climate change through ozone effects on the land-carbon sink, *Nature*, *448*(7155), 791–794, doi:10.1038/nature06059.

Spivakovsky, C. M., et al. (2000), Three-dimensional climatological distribution of tropospheric OH: Update and evaluation, *J. Geophys. Res.*, *105*(D7), 8931–8980, doi:10.1029/1999JD901006.

Torres, O., Z. Chen, H. Jethva, C. Ahn, S. R. Freitas, and P. K. Bhartia (2010), OMI and MODIS observations of the anomalous 2008–2009 Southern Hemisphere biomass burning seasons, *Atmos. Chem. Phys.*, *10*(8), 3505–3513.

Ward, D. E., W. M. Hao, R. A. Susott, R. E. Babbitt, R. W. Shea, J. B. Kauffman, and C. O. Justice (1996), Effect of fuel composition on combustion efficiency and emission factors for African savanna ecosystems, *J. Geophys. Res.*, *101*(D19), 23569–23576, doi:10.1029/95JD02595.

van der Werf, G. R., J. T. Randerson, L. Giglio, G. J. Collatz, P. S. Kasibhatla, and A. F. Arellano Jr. (2006), Interannual variability in global biomass burning emissions from 1997 to 2004, *Atmos. Chem. Phys.*, *6*(11), 3423–3441, doi:10.5194/acp-6-3423-2006.

van der Werf, G. R., J. T. Randerson, L. Giglio, G. J. Collatz, M. Mu, P. S. Kasibhatla, D. C. Morton, R. S. DeFries, Y. Jin, and T. T. Van Leeuwen (2010), Global fire emissions and the contribution of deforestation, savanna, forest, agricultural, and peat fires (1997–2009), *Atmos. Chem. Phys.*, *10*(23), 11707–11735, doi:10.5194/acp-10-11707-2010.

Wooster, M. J., P. H. Freeborn, S. Archibald, C. Oppenheimer, G. J. Roberts, T. E. L. Smith, N. Govender, M. Burton, and I. Palumbo (2011), Field determination of biomass burning emission ratios and factors via open-path FTIR spectroscopy and fire radiative power assessment: Headfire, backfire and residual smouldering combustion in African savannahs, *Atmos. Chem. Phys.*, *11*(22), 11591–11615, doi:10.5194/acp-11-11591-2011.

Yokelson, R. J., D. W. T. Griffith, and D. E. Ward (1996), Open-path Fourier transform infrared studies of large-scale laboratory biomass fires, *J. Geophys. Res.*, *101*(D15), 21067–21080, doi:10.1029/96JD01800.

Yokelson, R. J., R. Susott, D. E. Ward, J. Reardon, and D. W. T. Griffith (1997), Emissions from smoldering combustion of biomass measured by open-path Fourier transform infrared spectroscopy, *J. Geophys. Res.*, *102(*D15), 18865–18877, doi:10.1029/97JD00852.

Yokelson, R. J., I. T. Bertschi, T. J. Christian, P. V. Hobbs, D. E. Ward, and W. M. Hao (2003), Trace gas measurements in nascent, aged, and cloud-processed smoke from African savanna fires by airborne Fourier transform infrared spectroscopy (AFTIR), *J. Geophys. Res.*, *108*(D13), 8478, doi:10.1029/2002JD002322.

Yokelson, R. J., T. J. Christian, T. G. Karl, and A. Guenther (2008), The tropical forest and fire emissions experiment: Laboratory fire measurements and synthesis of campaign data, *Atmos. Chem. Phys.*, *8*(13), 3509–3527.

Yokelson, R. J., I. R. Burling, S. P. Urbanski, E. L. Atlas, K. Adachi, P. R. Buseck, C. Wiedinmyer, S. K. Akagi, D. W. Toohey, and C. E. Wold (2011), Trace gas and particle emissions from open biomass burning in Mexico, *Atmos. Chem. Phys.*, *11*, 6787–6808, doi:10.5194/acp-11-6787-2011

Yurganov, L. N., et al. (2011), Satellite- and ground-based CO total column observations over 2010 Russian fires: Accuracy of top-down estimates based on thermal IR satellite data, *Atmos. Chem. Phys.*, *11*(15), 7925–7942, doi:10.5194/acp-11-7925-2011.